UNIVERSIDADE DA BEIRA INTERIOR
Ciências

Desenvolvimento de uma nova membrana bioativa para o tratamento de lesões da pele

Rosa Maria Saraiva Sequeira

Dissertação para obtenção do Grau de Mestre em
Biotecnologia
(2º ciclo de estudos)

Orientador: Professor Doutor Ilídio Joaquim Sobreira Correia
Co-orientador: Mestre Sónia Alexandra Pereira Miguel

Covilhã, junho de 2019

"O valor das coisas não está no tempo que elas duram, mas na intensidade com que acontecem. Por isso, existem momentos inesquecíveis, coisas inexplicáveis e pessoas incomparáveis." **Fernando Pessoa**

Para as minhas pessoas preferidas: pais e irmãos

Agradecimentos

Durante este último ano do meu mestrado, foram muitas as pessoas que contribuíram para a realização deste trabalho, a quem quero desde já agradecer.

Em primeiro lugar, gostaria de agradecer ao professor Ilídio Correia por me ter recebido no seu grupo de investigação, e me ter facultado os recursos necessários para que conseguisse desenvolver este trabalho. Agradeço a sua orientação ao longo deste ano, os seus conselhos na hora certa, a sua exigência, a sua preocupação e a sua boa disposição, que promoveram a realização deste trabalho com sucesso.

À minha co-orientadora, Mestre Sónia Miguel queria agradecer por ter sido o meu grande pilar no laboratório desde o início até ao fim desta jornada. Agradeço-lhe o seu apoio diário, a sua amizade, todos os ensinamentos, toda a paciência, preocupação e toda a motivação que me transmitiu em determinadas alturas. Não existem "obrigadas" que cheguem para toda a sua ajuda incansável, que jamais esquecerei.

Ao André, Duarte e Elisabete agradeço por toda a boa disposição presente todos os dias e o espírito entreajuda.
Às "frozens" e à "piki" Telma agradeço por todos os momentos de descontração, por todas as brincadeiras e risadas diárias, que sem dúvida contribuíram para um bom ambiente de trabalho e que fizeram com que este ano passasse tão rápido. Em especial, agradeço à Cátia Sol por ter sido uma enorme surpresa neste ano, desde toda a sua ajuda incansável, motivação, preocupação e à amizade que se criou.
Aos meus amigos mais próximos, que me acompanharam durante a vida académica e aos outros amigos de longa-data agradeço por toda a amizade, apoio, compreensão e por todos os momentos memoráveis que me proporcionaram risos e sorrisos, e por todos aqueles em que foi preciso um abraço mais forte. Em especial agradeço à Telma e à Isabel, por me mostrarem que a verdadeira amizade perdura a longas distâncias.

À minha família, agradeço do fundo do coração por "voarem" comigo em cada etapa. Aos meus queridos pais agradeço todo o amor incondicional, todos os conselhos, toda a força inigualável que me transmitem todos os dias, e por acreditarem em mim mesmo quando eu não acredito. À minha irmã e irmão agradeço por serem um exemplo para mim, por toda a alegria que me causam, por me apoiarem sempre em cada decisão e me terem dado o melhor presente deste último ano: 3 sobrinhas, que me fazem ser a tia mais babada e mais orgulhosa.

Por fim, agradeço ao Daniel, meu colega de laboratório e namorado por iluminar os meus dias com positivismo e carinho. Agradeço por ter madrugado vários dias para me fazer companhia

no laboratório mesmo até horas incertas, por acreditar em mim e me motivar todos os dias durante toda esta aventura.

Bem-haja a todos!

Resumo

A pele é o órgão mais externo, que atua como uma barreira protetora, e está envolvida na regulação da temperatura corporal e na manutenção da homeostase dos líquidos. Diariamente a pele está exposta a diferentes agentes que podem causar diferentes tipos de lesões (queimaduras, intervenções cirúrgicas e/ou feridas crónicas). Quando ocorre uma lesão na pele, é crucial que esta seja imediatamente revestida com o intuito de proteger a área lesada contra os agentes externos. Na atualidade, são usadas diversas terapias para o tratamento das lesões, no entanto nenhuma delas é capaz de restabelecer completamente a estrutura e funções da pele. Neste contexto, na área de Engenharia de Tecidos têm sido produzidas diferentes matrizes poliméricas e biocompatíveis capazes de reproduzir a estrutura nativa da pele e de promover a adesão e proliferação celular. Entre os diferentes tipos de materiais usados até ao momento, as membranas nanofibrosas produzidas por eletrofiação têm apresentado resultados promissores nesta área. Desta forma, o plano de trabalhos desenvolvido neste mestrado teve como principal objetivo a produção e caracterização de uma membrana constituída por nanofibras. A membrana foi produzida recorrendo à técnica de eletrofiação, usando uma mistura de álcool polivinílico e lisina, a qual foi funcionalizada com dois tipos de biomoléculas: ibuprofeno (molécula com propriedades anti-inflamatórias) e óleo de lavanda (molécula com propriedades antibacterianas). O ibuprofeno foi incorporado nas nanofibras através da técnica de *blend electrospinning*, a fim de promover uma libertação controlada e sustentada durante a fase de inflamação (1-3 dias após a lesão), enquanto que o óleo de lavanda foi incorporado na superfície das membranas por adsorção física, com o objetivo de obter uma libertação inicial e desta forma evitar a ocorrência de infeção no local da lesão. Os resultados obtidos revelaram que as membranas apresentam propriedades morfológicas, mecânicas e biológicas apropriadas para serem aplicadas no tratamento de lesões cutâneas. Além disso, as membranas revelaram resultados promissores para serem usadas como sistemas de entrega de biomoléculas, uma vez que a libertação de ibuprofeno ocorre de uma forma controlada e sustentada (apresentando um pico de libertação após 24h de incubação). O óleo de lavanda apresentou um pico inicial, após 4h de incubação. Os perfis de libertação apresentados pela membrana permitirão a sua aplicação para controlar o processo inflamatório e ainda evitar a ocorrência de infeções cutâneas. Por outro lado, os ensaios antimicrobianos realizados demonstraram que as membranas funcionalizadas com óleo de lavanda apresentam uma excelente atividade antibacteriana contra a *S.aureus* e a *P.aeruginosa*.

Palavras-chave

Ibuprofeno; membranas eletrofiadas; óleo de lavanda; regeneração da pele; sistemas de entrega de biomoléculas.

Resumo alargado

A pele é o maior órgão do corpo humano, possui uma área aproximada de 2 m^2 e constitui cerca de 8% da sua massa total. As principais funções deste órgão incluem a proteção contra agentes externos, regulação da temperatura corporal, prevenção contra a desidratação e manutenção da homeostase dos fluídos corporais. Contudo, a integridade deste órgão é frequentemente comprometida por traumas (lacerações, queimaduras, procedimentos cirúrgicos) ou patologias (diabetes). Consoante o tipo e a duração do processo de cicatrização de feridas, as lesões da pele podem ser classificadas como agudas ou crónicas. A cicatrização de feridas é realizada através de uma cascata de eventos complexos e dinâmicos, que incluem coagulação, inflamação, migração celular, proliferação, síntese de deposição da matriz extracelular, angiogénese, fibroplasia, epitelização, contração e remodelação. Após ocorrer uma lesão, a pele necessita de ser imediatamente revestida de forma a diminuir a dor, a contaminação, o risco de infeção e a promover o mais rapidamente o restabelecimento da sua integridade estrutural.

Atualmente, os enxertos (nomeadamente auto e aloenxertos) são as abordagens terapêuticas mais usadas para o tratamento de feridas. No entanto, estes tipos de terapias apresentam diversas limitações: requerem longos períodos de internamento; disponibilidade limitada; têm associado um elevado risco de rejeição imunológica. De modo a ultrapassar estas limitações, os investigadores da área da Engenharia de Tecidos têm desenvolvido vários revestimentos cutâneos com o objetivo de melhorar/acelerar o processo de cicatrização de feridas. Na atualidade existem diversos substitutos de pele que são classificados de acordo com a camada de pele que se pretende regenerar. Assim, existem os substitutos epidérmicos, dérmicos e dermo-epidérmicos, que são produzidos com polímeros naturais e/ou sintéticos, sendo que alguns deles podem conter células no seu interior. No entanto, estas abordagens são demasiado caras, apresentam risco de rejeição imunológica e não conseguem restabelecer na íntegra todas as funções da pele nativa.

Entre os diferentes tipos de materiais que têm sido usados para promover a cicatrização de feridas, as membranas produzidas por eletrofiação têm captado o interesse dos investigadores. Estas membranas possuem uma estrutura fibrosa muito semelhante à estrutura da matriz extracelular da pele nativa, uma elevada porosidade que é fundamental para permitir a infiltração celular e troca de gases/nutrientes. Além disso, os exsudados das feridas podem ser eficazmente absorvidos devido ao elevado rácio área/volume apresentado por estas membranas, ajudando a manter o ambiente húmido no local da lesão. Por outro lado, estas estruturas nanofibrosas podem ser facilmente funcionalizadas com diferentes tipos de biomoléculas para lhe conferir propriedades antibacterianas e/ou melhorar o processo de cicatrização. Assim, as biomoléculas mais incorporadas nas nanofibras são moléculas com

propriedades antibacterianas (como antibióticos, nanopartículas de prata e extratos naturais) e moléculas com atividade biológica (por exemplo, fatores de crescimento, vitaminas e moléculas anti-inflamatórias).

Adicionalmente, as moléculas podem ser incorporadas recorrendo ao uso de diferentes técnicas, desde a mistura direta das biomoléculas na solução polimérica até à funcionalização da superfície da membrana após a sua produção. Desta forma, o perfil de libertação das biomoléculas poderá ser adaptado às necessidades específicas da fase (homeostase, inflamação, proliferação ou remodelação) do processo de cicatrização.

No presente trabalho foi efetuada a produção e caracterização de uma membrana nanofibrosa. O álcool polivinílico e a lisina foram usados na eletrofiação da membrana de modo a combinar as excelentes propriedades mecânicas do polímero sintético com as propriedades biológicas do aminoácido. Posteriormente, a membrana de álcool polivinílico_lisina foi funcionalizada com dois tipos de biomoléculas: ibuprofeno (molécula anti-inflamatória) e óleo de lavanda (molécula com propriedades antibacterianas). O ibuprofeno foi incorporado nas fibras através da técnica de *blend electrospinning*, com o objetivo de ser libertado de forma controlada e sustentada até à fase inflamatória (1-3 dias após a lesão). Por outro lado, o óleo de lavanda foi incorporado na superfície das membranas através de adsorção física, de forma a ser libertado no início do processo de cicatrização e desta forma evitar a ocorrência de infeção no local da lesão.

Os resultados obtidos neste estudo revelaram que as membranas apresentam propriedades morfológicas, mecânicas e biológicas apropriadas para serem aplicadas no tratamento de lesões cutâneas. O ibuprofeno foi libertado de forma controlada e sustentada (apresentando um pico de libertação após 24h de incubação). Por outro lado, o perfil de libertação do óleo de lavanda apresentou um pico inicial, após 4h de incubação, o que contribui para um ambiente asséptico no local da lesão. Desta forma, esta membrana permitirá controlar o processo inflamatório e ainda evitar a ocorrência de infeções cutâneas, através da libertação 'programada' de ambas as biomoléculas. Os ensaios antimicrobianos demonstraram que as membranas funcionalizadas com óleo de lavanda apresentaram excelente atividade antibacteriana contra a *S.aureus* e a *P.aeruginosa*. O sistema produzido neste estudo poderá atuar como sistema de entrega de biomoléculas, e simultaneamente fornecer suporte temporário à adesão e proliferação celular. No futuro, as membranas produzidas serão avaliadas em estudos *in vivo* com o objetivo de avaliar a sua aplicabilidade no tratamento de feridas.

Abstract

The skin is the outermost organ of the body and its acts as a protective barrier. Furthermore, skin is also responsible for the regulation of the body temperature and also for the maintenance of homeostasis. However, different types of injuries (burns, surgical interventions and/or chronic wounds), affect skin structure and functions. When a skin injury occurs, it is crucial to cover the wound site as soon as possible to provide protection against external agents. Despite this, there are several therapeutic strategies available for the treatment of skin injuries, none of them is able to restore all morphological and biological properties of the skin. In this context, Tissue Engineering researchers aim to produce polymeric and biocompatible matrices capable of reproducing the native structure of the skin, as well as, promote cell adhesion and proliferation. Among the different types of materials produced so far, the nanofibrous membranes produced by the electrospinning technique have demonstrated promising properties to be used in wound dressing applications. Thus, the work presented in this dissertation intended to produce and characterize a nanofibrous membrane. Poly(vinyl alcohol) (PVA) and lysine (Lys) were selected to produce the membrane, then functionalized with ibuprofen (IBP) (an anti-inflammatory molecule), and lavender oil (LO) (an antibacterial molecule). The IBP was incorporated into the nanofibers through an electrospinning blend technique, in order to be released in controlled and sustained fashion during the inflammatory phase (1-3 days after injury), while the LO was incorporated into the membrane' surface through physical adsorption technique, to allow an initial burst release which is essential to prevent the occurrence of infections at wound site.

In this way, the produced membrane will allow to control the inflammatory process and avoid the occurrence of skin infections. Indeed, the antimicrobial assays demonstrated that LO functionalized membranes exhibited excellent antibacterial activity against *S.aureus* and *P.aeruginosa*. All the gathered data revealed that the PVA_Lys membrane incorporated with IBP and LO possess the suitable morphological, mechanical and biological properties to be used as wound dressing.

Keywords

Biomolecule delivery systems; electrospun membranes; ibuprofen; lavender oil; skin regeneration.

List of publications

Articles published in international peer reviewed journals:

Miguel, S.P., Sequeira, R.S., Moreira, A.F., Cabral, C.S.D., Mendonça, A.G., Ferreira, P., Correia, I.J. (2019). An overview of electrospun membranes loaded with bioactive molecules for improving the wound healing process. *European Journal of Pharmaceutics and Biopharmaceutics*.139,1-22.

Miguel, S.P., Simões, D., Moreira, A.F., Sequeira, R.S., Correia, I.J. (2018). Production and characterization of electrospun silk fibroin based asymmetric membranes for wound dressing applications. *International Journal of Biological Macromolecules*. 121, 524-535.

Articles submitted for publication in international peer reviewed journals:

Sequeira, R.S., Miguel, S.P., Cabral, C.S.D., Moreira, A.F., Correia, I.J. (2019). Development of a Poly(vinyl alcohol)/Lysine electrospun membrane-based drug delivery system for improving the skin regeneration.

Contents

Chapter I – Introduction

1.Introduction 2
1.1. Skin structure and functions 2
1.1.1. Epidermis 2
1.1.2. Dermis 4
1.1.3. Hypodermis 5
1.1.4. Skin appendages 5
1.2. Wounds 5
1.2.1. Wound healing process 7
1.2.1.1. Hemostasis 7
1.2.1.2. Inflammation 7
1.2.1.3. Cell migration and proliferation 7
1.2.1.4. Remodelling 8
1.3. Tissue Engineering and skin substitutes 9
1.4. Electrospun membranes 14
1.4.1. Electrospinning set-up used to produce the electrospun membranes 14
1.4.2. Polymers used to produce electrospun membranes 15
1.4.2.1. Poly(vinyl alcohol) 16
1.4.2.2. L- Lysine 17
1.4.3. Electrospun membranes as drug delivery systems 17
1.4.3.1. Ibuprofen 19
1.4.3.2. Lavender oil 19
1.5. Aims 21

Chapter II - Materials and Methods

2. Materials and Methods 23
2.1. Materials 23
2.2. Methods 23
2.2.1. Production of electrospun membranes 23
2.2.2. Characterization of the membranes' morphology 24
2.2.3. Attenuated total reflectance-Fourier transform infrared spectroscopy analysis 24
2.2.4. Characterization of the mechanical properties of the membranes 24

2.2.5. Evaluation of the membranes' porosity 25
2.2.6. Evaluation of membranes' wettability 25
2.2.7. Water vapor transmission rate (WVTR) 25
2.2.8. Evaluation of the swelling capacity of the produced membranes 26
2.2.9. Characterization of the biodegradation profile of the membranes 26
2.2.10. Evaluation of antioxidant capacity of the membranes 26
2.2.11. Evaluation of the encapsulation and loading efficiency of IBP and LO within membranes 27
2.2.12. *In vitro* IBP and LO release profile and analysis of the drug-release kinetics 27
2.2.13. Characterization of the biological properties of the produced membranes 28
2.2.13.1. Evaluation of cell viability and proliferation in contact with electrospun membranes 28
2.2.13.2. dsDNA quantification 28
2.2.13.3. Live/Dead assay 29
2.2.13.4. Characterization of cell proliferation through confocal microscopy analysis 29
2.2.14. Evaluation of the antimicrobial properties of the produced membranes 29
2.2.15. Characterization of biological properties of the membranes through SEM analysis 30
2.2.16. Statistical Analysis 30

Chapter III - Results and Discussion

3. Results and discussion 32
3.1. Characterization of the morphological and physicochemical properties of produced nanofibrous membranes 32
3.2. Characterization of the membranes' mechanical properties 34
3.3. Determination of the total porosity of the membranes 35
3.4. Evaluation of the weight loss of the membranes 36
3.5. Characterization of electrospun membranes' swelling profile 37
3.6. Determination of water vapor transmission rate of membranes 37
3.7. Characterization of membranes' wettability through the measurement of water contact angles 38
3.8. Evaluation of the antioxidant activity of the membranes 39
3.9. Characterization of drug release profiles of IBP and LO from nanofibers 40
3.10. Characterization of biological properties of the electrospun membranes 41
3.11. Evaluation of antimicrobial properties of the electrospun membranes 46

Chapter IV - Conclusion and Future Perspectives

4. Conclusions and Future Perspectives 50

Chapter V - References

5. References 52
Appendix 64

List of Figures

Chapter I - Introduction

Figure 1. Schematic representation of the structure of the skin 2
Figure 2. Illustration of the layers and cellular components of the epidermis 4
Figure 3. Illustrative representation of the classification of the skin injuries according to the number of layers and area of skin affected 6
Figure 4. Illustrative representation of the main phases of the wound healing process 8
Figure 5. Representation of a tissue engineering strategy aimed to be used for the regeneration of a functional tissue 10
Figure 6. Representation of a conventional electrospinning apparatus, that is used to produce electrospun membranes. 15
Figure 7. Representation of chemical structure of PVA. 17
Figure 8. Representation of chemical structure of L-lysine 17
Figure 9. Illustration of the main strategies used to incorporate drugs into electrospun nanofibers 18
Figure 10. Representation of chemical structure of IBP 19
Figure 11. Representation of chemical structure of main component of LO (Linalool). 20
Figure 12. Schematic representation of the experimental setup used herein to produce the electrospun membranes-based drug delivery systems 21

Chapter III - Results and Discussion

Figure 13. Characterization of the electrospun membranes (PVA_Lys, PVA_Lys_IBP and PVA_Lys_LO) morphological features 33
Figure 14. ATR-FTIR analysis of the raw materials (A) and raw biomolecules (IBP and LO) and the produced electrospun membranes (B). 34
Figure 15. Characterization of the porosity (A), weight loss (B) and swelling profile at pH 5 (C) and at pH 8 (D) of the PVA_Lys, PVA_Lys_IBP and PVA_Lys_LO membranes 36
Figure 16. Characterization of physicochemical properties of the produced membranes 39
Figure 17. Optical microscopic images of NHDF cells cultured in the presence of the produced membranes (PVA_Lys, PVA_Lys_IBP and PVA_Lys_LO) 42
Figure 18. Characterization of the electrospun membranes'biocompatibility 43
Figure 19. Fluorescence microscopic images of Live/Dead assay 45
Figure 20. CLSM images of NHDF cultured on the electrospun membranes' surface 46
Figure 21. Evaluation of the produced membranes antibacterial activity 47
Figure 22. SEM images of control, PVA_Lys, PVA_Lys_IBP and PVA_Lys_LO membranes incubated with *S.aureus* and *P.aeruginosa* 48

List of Tables

Chapter I – Introduction

Table 1. Examples of skin substitutes available in the market to be used in the clinic. 12
Table 2. Description of the advantages and disadvantages of the natural and synthetic polymers..... 16

Chapter III - Results and Discussion

Table 3. Mechanical properties exhibited by the produced membranes 35
Table 4. Regression coefficients obtained by applying the mathematical models to fit the release of IBP and LO from the PVA_Lys nanofibrous membrane at pH 5 and pH 8. 41

Acronyms

ATR-FTIR	Attenuated total reflectance-Fourier transform infrared spectroscopy
bAg	Biosynthesized silver nanoparticle
CLSM	Confocal laser scanning microscopy
COX	Cyclooxygenase
DMEM-F12	Dulbecco's modified eagle's medium
DPPH	2,2-diphenly-1-picrylhydrazyl
EE	Encapsulation efficiency
EO	Essential oil
ECM	Extracellular matrix
EDTA	Ethylenediaminetetraacetic acid
FBS	Fetal bovine serum
GFs	Growth factors
LE	Loading efficiency
LO	Lavender oil
Lys	Lysine
MTS	3-(4,5-dimethylthiazol- 2-yl)-5-(3-carboxymethoxyphenyl)-2 (4-sulfophenyl)-2H-tetrazolium salt
NSAID	Non-steroidal anti-inflammatory
NHDF	Normal human dermal fibroblasts
P.aeruginosa	*Pseudomonas aeruginosa*
PBS	Phosphate-buffered saline solution
PMS	Phenazine methosulfate
PCL	Polycaprolactone
PEO	Polyethylene oxide
PLA	Polylactic acid
PLGA	Poly(lactic-co-glycolic acid)
PU	Polyurethane
PVA	Poly(vinyl alcohol)
ROS	Reactive oxygen species
RT	Room temperature
S.aureus	*Staphylococcus aureus*
SEM	Scanning electron microscopy
WCA	Water contact angle
WVTR	Water vapor transmission rate

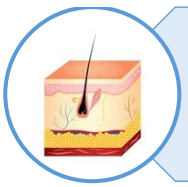

Chapter I - Introduction

1.Introduction

1.1. Skin structure and functions

Skin is the largest organ of the human body, covering about 1.7 m^2 and comprising approximately 8% of the total body mass. Furthermore, it is the outermost organ of the body, providing a barrier that protects inner organs from microbial pathogens, mechanical and chemical insults [1, 2]. In addition, the skin is also involved in fluid homeostasis maintenance, thermoregulation, immune surveillance, sensory detection, and dehydration prevention [3]. It contains three anatomical distinct layers known as epidermis, dermis, and hypodermis (as illustrated in Figure 1) [4]. Skin also display appendages like nails, hair follicles, sweat and sebaceous glands, nerves, that are found in the epidermis and dermis where they play distinct functions [5].

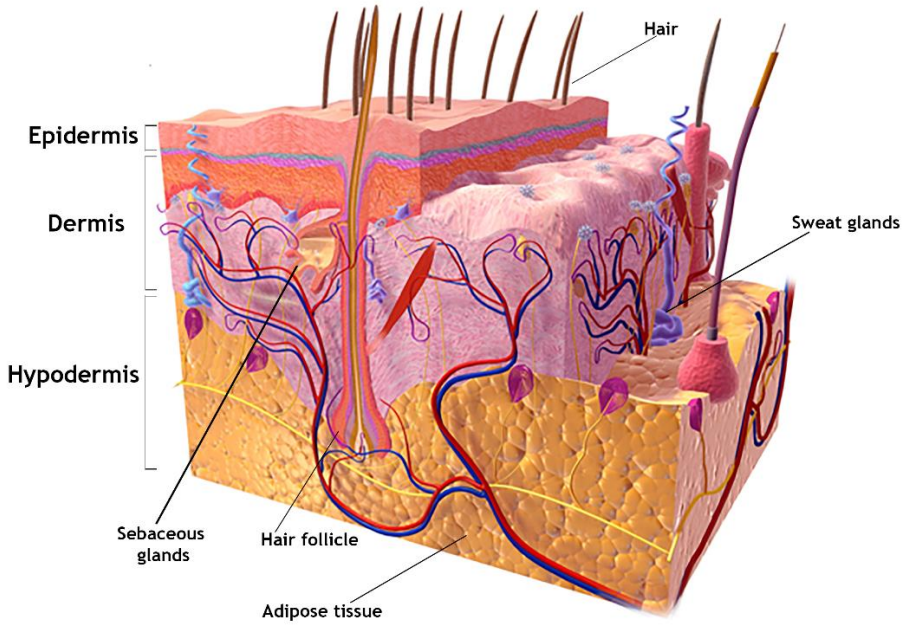

Figure 1. Schematic representation of the structure of the skin (adapted from [6]).

1.1.1. Epidermis

Epidermis is the outermost layer of the skin and it acts as impermeable boundary between the environment and the body, that avoids the loss of fluids and the occurrence of infections. Furthermore, it is a multilayered cellular structure with few or no extracellular matrix (ECM) and it is avascular [1]. Keratinocytes are the most abundant cell type in epidermis (95%), that are able to undergo self-renewal through a continuous process of proliferation, differentiation and cell death [2]. Keratinocytes differentiation process enables the compartmentalization of

epidermis into five distinct cell layers, known as *strata basale*, *spinosum*, *granulosum*, *lucidum*, and *corneum* (from the deepest to the most superficial), as represented in Figure 2 [2, 4].

The *stratum basale* is composed of several layers containing cuboidal nucleated epithelial cells, known as skin stem cells [7, 8]. These stem cells have a high self-renewal capacity and they migrate to the *stratum spinosum*, where the keratinization process begins. At this stage, the cells suffer shape changes, lose their cytoplasm and start to synthesize keratin. In the *stratum granulosum*, the keratinocytes, due to the differentiation process, accumulate lipid granules, which are essential for the maintenance of a water barrier [8, 9]. Morphologically, the keratinocytes present in this layer become flat and spread. In the *strata lucidum* and *corneum*, cells enter into the programmed cell death process and all of the cytoplasmic organelles are degraded [10]. The *stratum corneum* is the most external layer of the epidermis, representing the final stage of keratinocyte differentiation. This layer is composed of differentiated dead keratinocytes interspersed with intercellular lipids (mainly ceramides and sphingolipids). The keratinized *stratum corneum* is in direct contact with the environment, providing a main barrier to prevent water loss and penetration of harmful agents. Normally, the keratinocytes migration from the *stratum basale* to the outer *stratum corneum* takes approximately 28 days. Additionally, the epidermis is also composed by melanocytes (3%) which are responsible for its pigmentation. Merkel cells (0.5%) acts as mechanosensory receptors, and Langerhans cells (2%) are involved in the skin immune defense system [5, 9].

The epidermis is connected to the underlying dermis, through basement membrane, at the dermal-epidermal junction. The basement membrane is composed of two main layers: lamina lucida (the layer that is closer to the epidermis, which is comprised of laminin, integrins, entactins, and dystroglycans) and lamina densa (a sheet-like structure composed mainly by collagen type IV) [1, 9, 10].

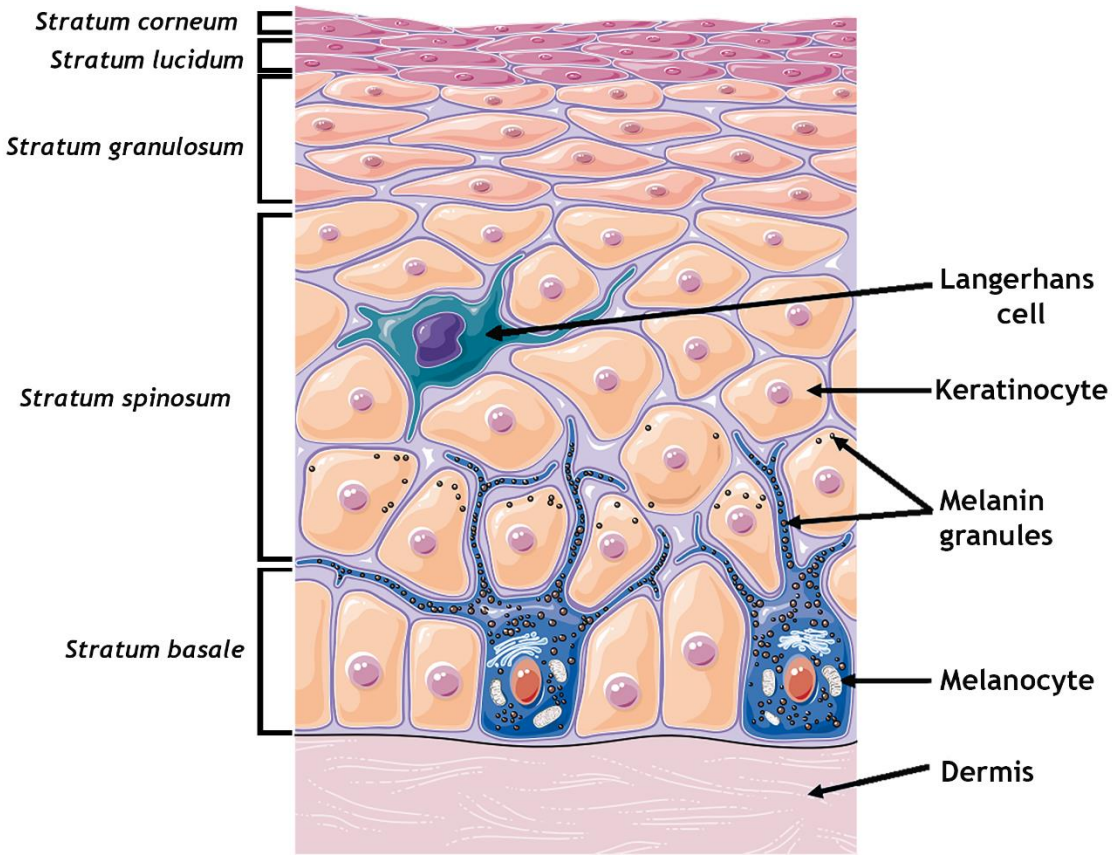

Figure 2. Illustration of the layers and cellular components of the epidermis. The outermost layer of the epidermis, the *stratum corneum*, is fundamental to avoid microorganisms' penetration and protect the skin from environmental insults. The other *strata* (*lucidum*, *granulosum*, *spinosum* and *basale*) are fundamental for the remodelling of the *stratum corneum*. The epidermis also contains Langerhans cells and melanocytes (adapted from [11]).

1.1.2. Dermis

The dermis layer is located between epidermis and hypodermis layers, and it displays a thickness of 3-5 mm. This layer supplies energy and nutrition to the overlying epidermis, since it is enriched by blood and lymphatic vessels, as well as nerve fibers. On the other side, the dermis' cellular components include fibroblasts, adipocytes, macrophages and mast cells [2, 4]. Fibroblasts are the most abundant cell type present in this layer and they are responsible for the production of ECM components (*e.g.* collagen, fibrin, fibronectin, elastin, proteoglycans, glycosaminoglycans and remodelling enzymes) [1, 2]. Collagen and elastic fibers provide support and elasticity to the skin [1-3].

The dermis structure is organized into two different layers: the upper papillary dermis and the deeper reticular dermis [10]. The superficial papillary dermis is composed of thin fibers that are loosely arranged and contains blood vessels that supply nutrients, and remove waste products from the epidermis, as well as regulate the body temperature [1, 10]. Unlike, the deeper reticular dermis accounts for 80% of dermis and it is composed of dense collagen and

elastic fiber matrix, that provides strength and flexibility to the skin [9, 10]. Furthermore, the dermal layer also contains lymphatic vessels, nerve fibers, sweat and sebaceous glands [9].

1.1.3. Hypodermis

The hypodermis is the bottom layer of the skin, it is located below the dermis, and it is also known as subcutaneous tissue, that is involved in the connection between skin, bones and adjacent muscles [9]. This layer is mainly composed of adipose and connective tissues. In addition, the hypodermis is highly vascularized, provides blood vessels and nerves to the skin, and also contributes to the thermoregulatory and mechanical properties of the skin [9, 10].

1.1.4. Skin appendages

Skin is also composed of a variety of appendages such as nails, hair, sebaceous glands and sweat glands [9, 10, 12]. The nails are highly keratinized structures and provide physical protection to the end of the fingers and toes. In a similar way, the hair is also a keratinized structure, involved in the thermoregulation, physical protection, sensory activity, and social interactions [13, 14].

In turn, the sebaceous glands are holocrine glands responsible for sebum secretion. The lipid-hydrophobic nature of sebum provides waterproofing and moisturizing actions at the skin surface [13, 14]. The sweat glands are located within the dermis and they secrete sweat, which is fundamental for the thermoregulation and excretion of metabolites [12, 13].

1.2. Wounds

Wounds affect millions of people worldwide, being this pathology one of the major issues in modern health care systems [15]. A wound can be defined as a disruption of the structural and functional integrity of the skin, which can occur as a consequence of the physical, chemical, mechanical, and/or thermal damage [16, 17]. According to type and duration of the repair process, the wounds can be classified as acute or chronic [16].

Acute wounds result essentially from the surgical incisions, abrasions, and burns. Usually, this type of wounds heals completely within 8-12 weeks. In brief, acute wound healing is a timely ordered process that involves several events, which are regulated by mediators like platelets, inflammatory cells, cytokines, and growth factors (GFs) [18]. On the other side, the chronic wounds arise from tissue injuries that heal slowly or fail to heal due to repeated tissue insults or underlying physiological conditions like diabetes, persistent infections, or due to poor primary treatment [15, 16]. In this type of the wound, the healing process is not effective, and a state of pathologic inflammation arises, due to an excessive inflammation and bacterial colonization that usually occurs. Diabetic and pressure ulcers are some examples of chronic wounds [19].

Moreover, the wounds can be classified based on the number of layers and area of the skin affected. Therefore, they can be divided into superficial partial-thickness, deep partial thickness, and full thickness (as illustrated in Figure 3) [20, 21].

- **Superficial partial-thickness** – It affects the epidermis and superficial dermis, causing severe pain and epidermal blistering. The healing occurs through the epithelialization from the margins and the edge of the wound [1, 20, 21];

- **Deep partial-thickness** – These wounds affect a large area of skin, requiring a long period to heal. The scarring will be more pronounced in comparison to the superficial partial-thickness wounds [1, 20, 21];

- **Full-thickness** – It promotes a full destruction of dermis, epidermis and skin appendages. The heal of these wounds occurs through the contraction and the epithelialization processes, which occurs only from the edge of the wound. They require skin grafting and may lead to extensive scarring, cause mobility restrictions and cosmetic issues to the patients [1, 20, 21].

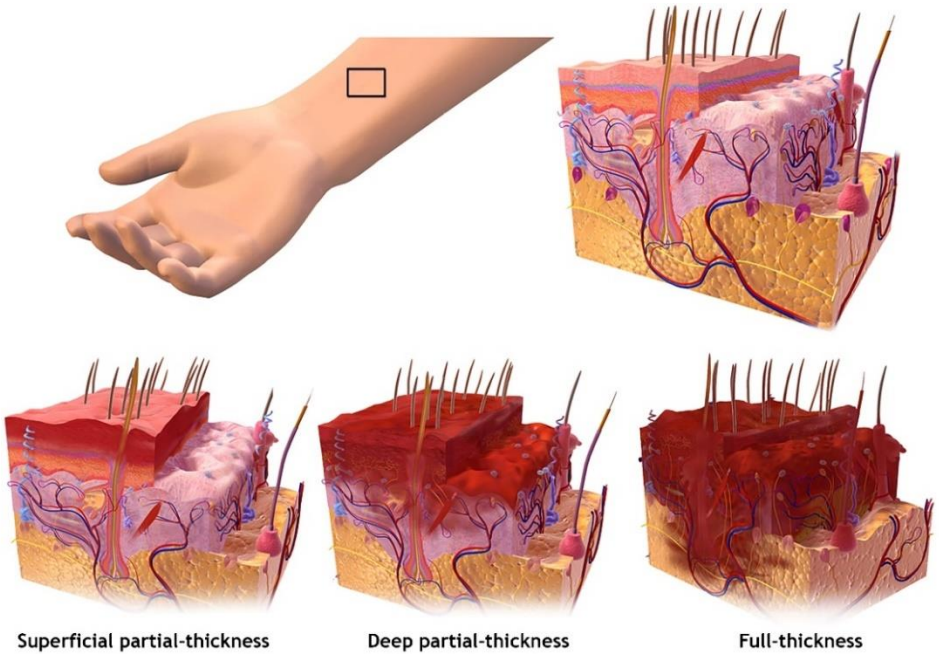

Figure 3. Illustrative representation of the classification of the skin injuries according to the number of layers and area of skin affected: superficial partial-thickness (affects the epidermis and superficial dermis); deep partial-thickness (affects a large area of skin, requiring a long treatment period); and full-thickness (occurs the full destruction of dermis, epidermis and skin appendages). Image was adapted from [6].

1.2.1. Wound healing process

The wound healing is a complex, extremely dynamic and interactive biological process, that includes a wide range of mechanisms such as coagulation, inflammation, cell migration, proliferation, contraction, deposition, angiogenesis, epithelialization, ECM synthesis, contraction and remodelling [22-25]. The wound healing process is known by involving essentially four phases: hemostasis, inflammation, cell migration/proliferation and remodelling (as illustrated in Figure 4) [15, 22-24].

1.2.1.1. Hemostasis

After the skin injury occurs, the hemostasis begins in order to prevent bleeding, through the production of a provisional matrix at wound site [22-24]. As consequence, the coagulation cascades are activated, leading to platelet aggregation. Such event will fill the tissue gap with a blood clot composed of fibrin, fibronectin, vitronectin, and thrombospondin. This clot acts as provisional support for the migration of leukocytes, keratinocytes, fibroblasts, endothelial cells and GFs [26].

1.2.1.2. Inflammation

The inflammatory phase occurs almost simultaneously with hemostasis, in order to clean the wound from the necrotic tissues and to prevent infection. In the initial stage of this phase, the neutrophils are recruited to the wound site, where they start the phagocytosis of bacteria, followed by their killing them through the release of enzymes and free radicals [23, 24]. After 2-3 days, blood monocytes differentiated into macrophages, that act as phagocytic cells in the later stages of inflammation. Further, the macrophages also secrete GFs (*e.g.* tumor necrosis factor-α (TGF-α), transforming growth factor-ß (TGF-ß), basic fibroblast growth factor (bFGF), platelet-derived growth factor (PDGF) and vascular endothelial growth factor (VEGF)), that are responsible for the proliferation of endothelial and smooth muscle cells and the ECM synthesis by fibroblasts, as well as, release of enzymes which aid in wound debridement [3, 23, 24, 27].

1.2.1.3. Cell migration and proliferation

The migration phase occurs at 2-10 days after skin injury and starts with the reestablishment of the skin. It is characterized by three important events, which involves the re-epithelialization, neovascularization and formation of granulation tissue [23, 24, 27]. This phase is initiated with the cell migration to the wound site, in order to promote the matrix production and formation of granulation tissue [23, 24].

Once in the wound, fibroblasts and myofibroblasts interact, proliferate and produce matrix proteins (*e.g.* fibronectin, elastin, hyaluronan, collagen, and proteoglycans). ECM is essential

for cell adhesion, growth and differentiation [23, 24]. Further, the fibroblasts also secrete FGF, that in combination with VEGF, secreted by platelets and neutrophils, act as angiogenic factors that stimulate endothelial cell proliferation and migration. In turn, the myofibroblasts are responsible for wound contraction, bringing the edges together [22-24].

1.2.1.4. Remodelling

Remodelling is the last phase of the wound healing, which starts 2-3 weeks after injury and lasts for months to years. The metalloproteinases secreted by fibroblasts, macrophages and endothelial cells are continuously replacing collagen type III by mature collagen type I, in order to induce a continuous remodelling of the ECM. Despite of the remodelling process continues for an extended period of time, the scar tissue does not achieve the strength of the native skin, neither present any skin appendages [23, 24, 26, 28].

In this phase, all the processes that were activated after injury, cease, due to degradation and replacement of immature ECM and to the apoptosis of different cell types (endothelial, fibroblasts and macrophages) resulting only in a mass composed of collagen and other ECM proteins [23, 24, 26].

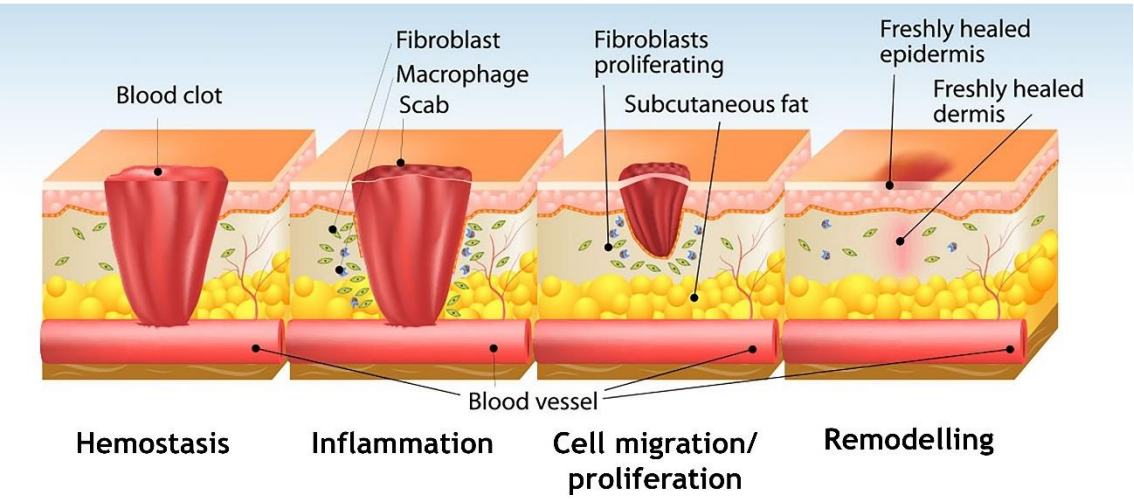

Figure 4. Illustrative representation of the main phases of the wound healing process. The hemostasis is characterized by the production of a clot, which acts as provisional ECM; Inflammatory phase is characterized by inflammatory cells infiltration; In the cell migration/proliferation phase, new fibroblasts and keratinocytes migrate into the wound, in order to re-establish and re-epithelize the dermal and epidermal layers; In remodelling phase, the wound contracts and an acellular scar tissue is formed. Image adapted from [29].

1.3. Tissue Engineering and skin substitutes

Skin loss occurs as a consequence of burns, namely thermal injuries. Accordingly to the World Health Organization, each year 180 000 deaths are attributed to burn injuries [30]. Only in United States, each year, there are 70 000 burn injuries [31] and 600 000 - 1 500 000 venous leg ulcers injuries [32]. The treatment of wounds costs nearly $20 billion annually in the US [31].

Nowadays, the gold standard therapy used for burns treatment is still the patients' own skin, known as autografts [1, 33]. In the case of severe skin injuries with an extensive damaged area, there are insufficient skin donor sites available in the patient and the solution is to use skin from human cadavers. However, the cadaveric skin provides only temporary coverage, due to host immune rejection. Further, the allografts present also a limited availability in skin banks, and have associated the risk of disease transmission [34, 35]. Another approach is the use of xenografts, which involves the transfer of tissue between different species, but it has also rejection problems associated [1, 36].

Hence, researchers from the Tissue Engineering area aim to develop therapeutic alternatives for skin regenerative purposes [10]. This interdisciplinary field applies the principles of engineering and life sciences toward the development of biologic substitutes that restore, maintain or improve tissue functions. The main strategy used in skin tissue engineering (as represented in Figure 5) involves the cell seeding in contact with biomaterials, which act as temporary scaffolds for cell adhesion and proliferation, in order to allow the restoring of the structures and functions of skin tissue [1, 37].

In this way, researchers working in the area of the skin tissue engineering have been searching for an ideal skin substitute that fills certain requirements like biocompatibility, biodegradability and non-immunogenicity. Skin substitutes also display antimicrobial properties, be nonadherent to the wound site, allow gaseous and fluid exchanges, absorb the excess of exudates, and support the handling during application. Moreover, it should also be able to improve the healing process, mimic the native skin environment, be comfortable and cost effective [1, 10].

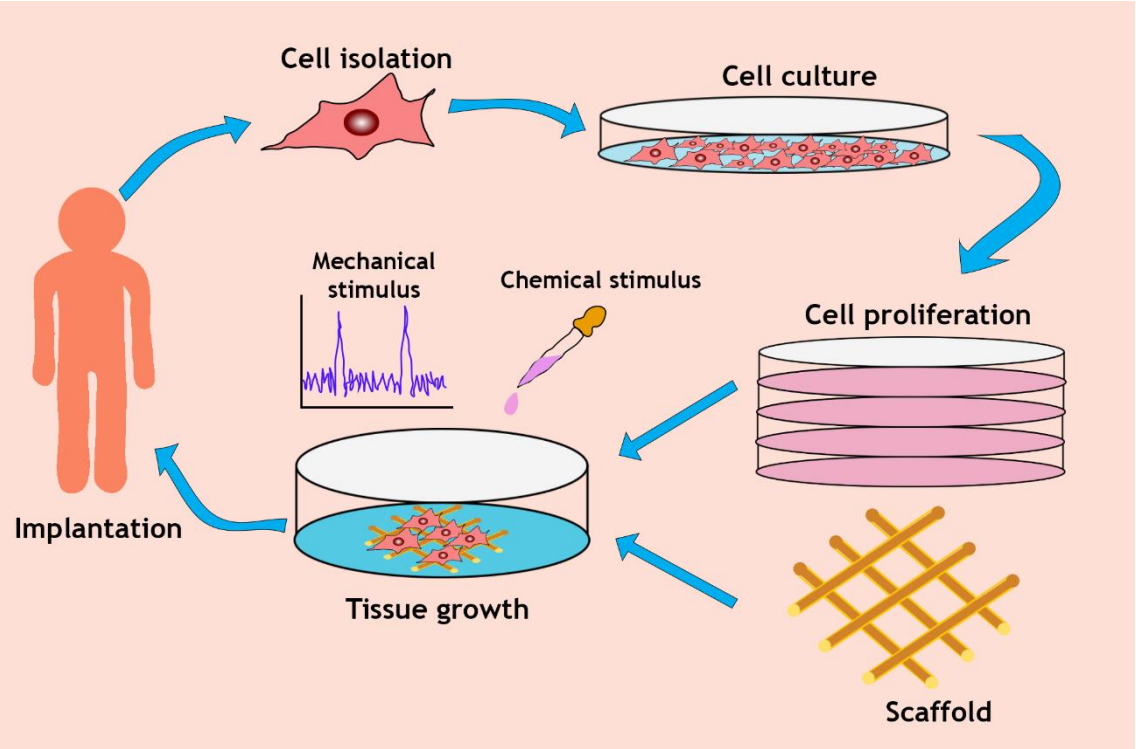

Figure 5. Representation of a tissue engineering strategy aimed to be used for the regeneration of a functional tissue. In this therapeutic approach, the cells are isolated from the patient, cultured and expanded *in vitro*. Subsequently, cells are seeded in contact with a scaffold, which act as provisional support for cell proliferation and under mechanical and chemical stimulus will promote the tissue growth. Ultimately, the construct is transplanted to the damaged tissue in order to restore its structure and function.

As result of this intense research, a variety of skin substitutes are already available in market and some of them are applied in the clinic (see Table 1) [1, 21, 34]. These skin bioengineered substitutes can be classified according to:

- Anatomical structure: epidermal, dermal, dermo-epidermal;
- Duration of the cover: permanent, semi-permanent, temporary;
- Type of the biomaterial used in their production: biological (autologous, allogeneic, xenogeneic) or synthetic (biodegradable, non-biodegradable);
- Cellular component: cellular or acellular.

Epidermal skin substitutes

Epidermal skin substitutes aim to repair the epidermis by promoting the re-epithelialization of the wound. In general, the key step to produce an epidermal substitute is the isolation of keratinocytes from a donor, followed by its subsequent *in vitro* cultivation on biocompatible substrates (*e.g.* bovine collagen, hyaluronic acid, etc.) [10, 34]. MySkin® is an example of epidermal skin substitute, that is composed of autologous keratinocytes that have been grown on a silicon support layer. On the other side, CellSpray consists of an aerosol of cell suspension that is directly sprayed on the wound site [38]. In general, the available skin epidermal substitutes are expensive, unable to treat full-thickness skin wounds and their production is time-consuming [10, 34].

Dermal skin substitutes

Dermal skin substitutes aim to treat/repair the damaged dermis. They provide mechanical stability, prevent the contraction of the wound and mimic the ECM structure and functions [1]. AlloDerm®, Integra® and Matriderm® are examples of acellular dermal substitutes available in the market [21, 34, 38]. AlloDerm® is an acellular dermal matrix that is applied for the treatment of full- and partial-thickness wounds. In turn, Dermagraft® is a cellular dermal substitute composed of a biodegradable polyglactin mesh, which is seeded with human neonatal fibroblasts [1, 21, 34].

Dermo-epidermal skin substitutes

Dermo-epidermal skin substitutes are the most advanced skin substitutes, since they mimic the native structure of the skin, possessing two main layers (epidermis and dermis) [10, 21, 34, 38]. These bilayers provide biological environment for skin regeneration and, simultaneously, act as temporary wound coverages. In general, keratinocytes and fibroblasts, either autologous or allogenic, are seeded on the top and bottom layer, respectively. Apligraf® contains of a bottom layer produced with bovine collagen type I incorporating allogeneic neonatal fibroblasts, combined with a top layer composed of cell suspension of allogeneic neonatal keratinocytes. On the other side, Orcel® is a tissue engineering construct that includes allogenic fibroblasts seeded into a bovine type I collagen sponge, on top of which keratinocytes are seeded to form a confluent layer [21]. Nevertheless, these bilayered skin substitutes are very expensive, present risk of infection to the patient and display weak mechanical properties [10, 21, 34, 38].

Table 1. Examples of skin substitutes available in the market to be used in the clinic.

	Product	Company	Cellularity	Biomaterials	Duration of skin substitute	References
Epidermal	Myskin®	Regenerys Ltd, Sheffield, UK	Cellular - autogenic keratinocytes	Plasma polymerized silicone film	Temporary	[39]
	Suprathel®	Polymedics Innovations GmbH, Denkendorf, Germany	Acellular	Copolymer of polylactide and ε-caprolactone	Temporary	[40]
Dermal	Alloderm®	LifeCell, Branchburg, New Jersey, USA	Acellular	Acellular dermis from cadaver	Temporary	[41]
	Integra®	Integra Life Science Corporation, Plainsboro, NJ, USA	Acellular	Silicone, bovine collagen type I, chondroitin-6-sulphate	Temporary	[42]
	Matriderm®	MedSkin Solutions Suelack AG, Billerbeck, Germany	Acellular	Bovine collagen matrix with α-elastin hydrolysate	Temporary	[43]
	Oasis®	Cook Biotech, Inc., West Lafayette, Indiana, USA	Acellular	Acellular extracellular matrix (porcine small intestine submucosa)	Temporary	[44]
	Dermagraft®	Advanced BioHealing, Inc., USA	Cellular – foreskin allogenic neonatal fibroblasts	Polyglactin mesh	Temporary	[45]
	TransCyte®	Advanced BioHealing Inc., La Jolla, CA, USA	Cellular - allogenic neonatal fibroblasts	Silicone, collagen coated nylon mesh	Permanent	[46]
	Hyalomatrix ®	Fidia Advanced Biopolymers, Padua, Italy	Acellular	Hyaluronan and silicone	Temporary	[47]
Dermo-epidermal	Apligraft®	Organogenesis, Inc., California, USA	Cellular- allogeneic neonatal fibroblasts and keratinocytes	Bovine collagen type I in the dermis layer	Temporary	[48]
	Karoskin	Karocell Tissue Engineering AB, Sweden	Cellular – dermal and epidermal cells	Human cadaver skin	Temporary	[21]
	Orcel®	Ortec Internation, Inc., New York, USA	Cellular -neonatal foreskin fibroblasts and keratinocytes	Bovine collagen sponge	Temporary	[49]

Despite of the tremendous efforts that have performed to develop advanced bioengineering skin substitutes, the commercially available skin substitutes yet present several limitations, like reduced vascularization, poor mechanical integrity, failure to become integrated, scarring and immune rejection [50].

Moreover, the development of engineered skin substitutes is a time-consuming process, involving 2-3 weeks of cell culture, before it is ready for grafting. Further, the available skin substitutes are mainly composed of fibroblasts and keratinocytes, and therefore, lack the ability to regenerate differentiated structures, like hair and sweat glands. Moreover, there is also a need to reduce the cost of current available skin substitutes, since the cost to cover 1% of body surface area with Epicel™ is more than $13 000 [1]. Therefore, further studies are needed to improve these bioengineered skin substitutes [1, 51].

In this way, the tissue engineering researchers have been developing a variety of wound dressings such as sponges, hydrogels, hydrocolloids, and nanofibrous membranes [15, 52]. These formulations have distinct properties that make them suitable for the treatment of a particular type of wound. For example, sponges exhibit a huge porosity, provide thermal insulation and sustain a moist environment at the wound site [53]. On the other side, hydrogels are characterized by their capacity to absorb high amounts of water within their 3D polymeric network, which allow them to provide a moist environment to the wound [54, 55]. Furthermore, hydrocolloids are easily removed by saline or sterile water, non-adherent, present high density and are painless dressings [56, 57]. In turn, the nanofibrous membranes are known by their structural similarity with the 3D architecture of native ECM. Moreover, their high surface-to-volume ratio and interconnected pores are crucial to promote cell proliferation, gas exchange, nutrient supply, and to control fluid loss [16, 58].

Among the different techniques used to produce the nanofibrous membranes (*e.g.* self-assembly, phase separation and electrospinning), the electrospinning has captured the attention of researchers due to its simplicity, cost-effectiveness and versatility. The features of the electrospun membranes will be described in more detail in following section.

1.4. Electrospun membranes

The electrospun membranes have been applied for drug delivery and regeneration of different tissues (*e.g.* skin, bone, cartilage and neural) [59, 60]. In terms of skin regeneration, the electrospun membranes possess distinct appealing properties that make them promising candidates for being applied in skin regeneration since they display the following properties [25, 61, 62]:

- **Mimic the structure of the ECM**
  The electrospun membranes nanofibers display diameters ranging from 50-500 nm, which are crucial for cell adhesion, migration, proliferation and differentiation. Further, these diameter values are very similar to that display by the collagen fibers found in skin ECM;
- **High surface-to-volume ratio**
  The high surface-to-volume ratio displayed by these membranes encourage cell attachment;
- **Interconnected porous structure**
  The high porous structure of electrospun membranes allows the absorption of wound exudates, gaseous and nutrients exchanges, providing a moist environment at wound site as well as prevent the wound dehydration;
- **Conformability**
  Electrospun membranes are able to adapt easily to the wound site with irregular architecture;
- **Functionality**
  The electrospun membranes can be functionalized with different bioactive compounds (*e.g.* antimicrobial and/or biological molecules) to improve/accelerate the healing process. The versatility of the electrospinning technique affords different types of drugs to be incorporated, as well as, it is possible to tailor the drug release profile according to the healing process demands.

1.4.1. Electrospinning set-up used to produce the electrospun membranes

Electrospinning is a simple technique that uses electrostatic forces to produce polymeric nanofibrous membranes with fibers displaying diameters ranging from 2 nm to several micrometers [25, 63].

In general, a conventional electrospinning setup (as illustrated in Figure 6) is composed of a syringe pump, a capillary needle connected to a syringe, a high-voltage power supply and a metal collector [25, 64]. During the electrospinning process, a high voltage is generated to produce an electrically charged jet of the polymeric solution that is projected to a collector

through the electrostatic forces. With the increasing of the intensity of electrical field, the charge induces an elongation of the droplet into a cone, known as Taylor Cone. Before reaching the collector, the jet undergoes a series of electrically driven instabilities and gradually thins in the air due to solvent evaporation [25, 59, 65].

During the electrospinning process, there are several parameters that have to be optimize and controlled, such as: properties of the precursor solution (*e.g.* conductivity, surface tension, viscosity, and solvent selection), processing variables (*e.g.* flow rate, voltage, and distance between capillary and the collector), and environmental conditions (*e.g.* temperature and humidity). These parameters will have a direct impact on the properties of the electrospun membranes, like the fibers' diameter, porosity, mechanical strength, among others [25, 66].

Further, the use of a stationary collector (as represented in Figure 6) allows the obtention of electrospun membranes with randomly orientated fibers, which is desirable to mimic the ECM of normal skin. However, the oriented fibers (desired for muscle and nervous tissue regeneration) can be obtained through the use of rotating collectors, where the rotation speed of the collector has direct influence on the diameter and the alignment of the produced fibers [25, 65, 66].

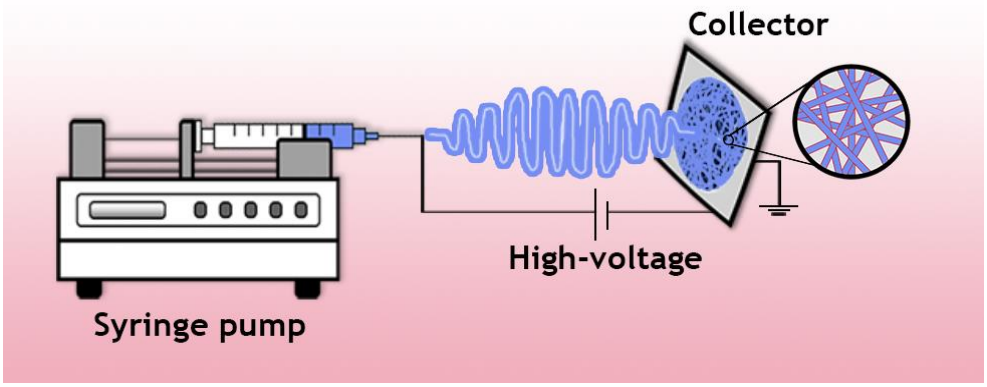

Figure 6. Representation of a conventional electrospinning apparatus, that is used to produce electrospun membranes.

1.4.2. Polymers used to produce electrospun membranes

Nowadays, the researchers have been combining synthetic with natural polymers to produce electrospun membranes [25, 59]. The synthetic polymers exhibit excellent mechanical properties, thermal stability and controlled degradation profiles. Although, their hydrophobic character and the absence of peptide sequences impair cell adhesion and proliferation [67]. On the other side, the surface of natural polymers can be easily recognized by cell surface receptors. Nevertheless, their high biodegradation rate and low mechanical properties can restrict their application [68]. In Table 2, the main advantages and disadvantages of the natural and synthetic polymers, as well as, examples of the polymers used in production of electrospun membranes are described.

Table 2. Description of the advantages and disadvantages of the natural and synthetic polymers. Examples of the polymers used in production of the electrospun membranes are also listed.

	Advantages	Disadvantages	Examples	References
Synthetic	-Biocompatible; -Suitable degradation profile; -Excellent mechanical properties; -Thermal stability.	-Absence of peptide sequences at their surfaces; -Weak cell interaction; -Hydrophobic character.	Polycaprolactone (PCL) Polylactic acid (PLA) Poly(lactic-co-glycolic acid) (PLGA) Polyurethane (PU) Poly(vinyl alcohol) (PVA)	[67, 69-73]
Natural	-Biocompatible; -Presence of peptide sequences at their surface; -Excellent cell interaction; -Hemocompatibility; -Antimicrobial, antioxidant and anti-inflammatory activity.	-Rapid degradation; -Poor processability; -Poor mechanical properties.	Collagen Gelatin Chitosan Silk fibroin Fibrinogen Hyaluronic acid	[69, 74-78]

1.4.2.1. Poly(vinyl alcohol)

PVA is a water-soluble, non-toxic and no-carcinogenic polymer synthesized through the polymerization of vinyl acetate to poly(vinyl acetate), followed by hydrolysis reaction of poly(vinyl acetate) to PVA (its chemical structure is represented in Figure 7) [73, 79, 80]. It is biodegradable, biocompatible and possess excellent mechanical properties and chemical resistance. Furthermore, PVA presents a high swelling capacity, which makes it appropriate for wound exudate absorption, as well as, for promoting a moist environment at the wound site. In fact, different researchers have already produced PVA-based electrospun membranes [56, 81]. For example, Kheradvar *et al*. combined PVA with silk fibroin and aloe vera to produce an electrospun membrane. The main results evidenced that these nanofibers are biocompatible, promote the fibroblasts adhesion, spreading and proliferation [82].

Moreover, Mohseni and their collaborators produced a wound dressing, through the incorporation of silver sulfadiazine (SSD) into PVA nanofibers in order to confer it antimicrobial properties. The results demonstrated that the PVA nanofibers incorporating SSD were able to avoid the microorganism growth, without impairing the eukaryotic cell proliferation [83]. Furthermore, Augustine *et al*. also developed an electrospun PVA membrane containing biosynthesized silver nanoparticle (bAg). The experimental results highlighted the good mechanical strength, excellent exudate uptake capacity, antibacterial activity, blood compatibility and cytocompatibility of the PVA electrospun membranes loaded with bAg [84].

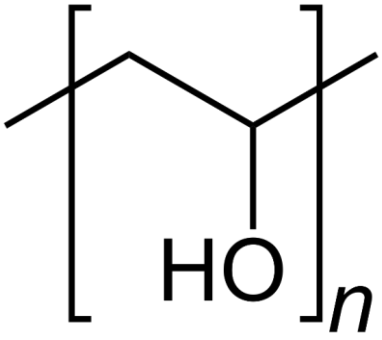

Figure 7. Representation of chemical structure of PVA.

1.4.2.2. L- Lysine

L-lysine (Lys) is a basic amino acid that possess three reactive groups (α-carboxyl group, α-amino group and ε-amino group) that enable its chemical modification (the chemical structure of Lys is represented in Figure 8) [85-87]. This amino acid is widely known by its ability to promote cell adhesion, proliferation and regeneration at biomaterial interface. The positively charged groups available on its surface enable a strong electrostatic interaction with the negatively charged compounds available at the cell membrane [88]. In fact, the researchers have been using Lys and their derivatives (poly-L-lysine) to cover the surface of culture dish to promote/encourage the cell adhesion [87, 89].

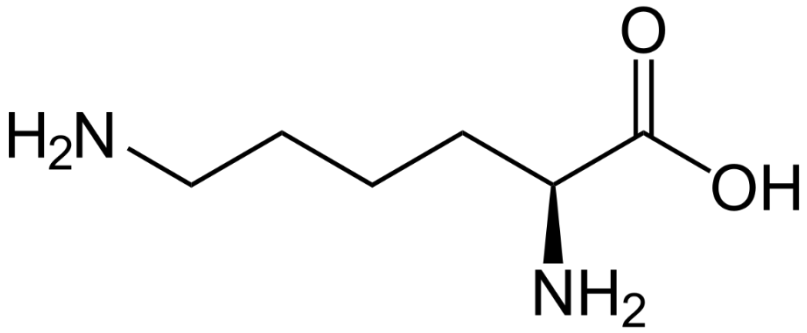

Figure 8. Representation of chemical structure of Lys.

1.4.3. Electrospun membranes as drug delivery systems

Besides of the intrinsic properties of electrospun membranes previously described, this type of the wound dressings can also act as drug delivery systems, allowing their functionalization with bioactive molecules that can enhance the wound healing process [52, 62, 90]. In fact, the combination of the high surface-to-volume ratio of the nanofibers with the possibility of selecting the most appropriate solvent for drug solubilization grant to these dressings a high loading capacity [15, 62, 91]. Furthermore, the nanofibers drug loading can be achieved by performing the incorporation of the biologic active agents by co-axial, multi-jet, emulsion, and secondary carrier electrospinning [25, 90, 92]. Moreover, the nanofibers surface can also be modified by physical adsorption, layer-by-layer assembly and chemical immobilization of biomolecules (as illustrated in Figure 9).

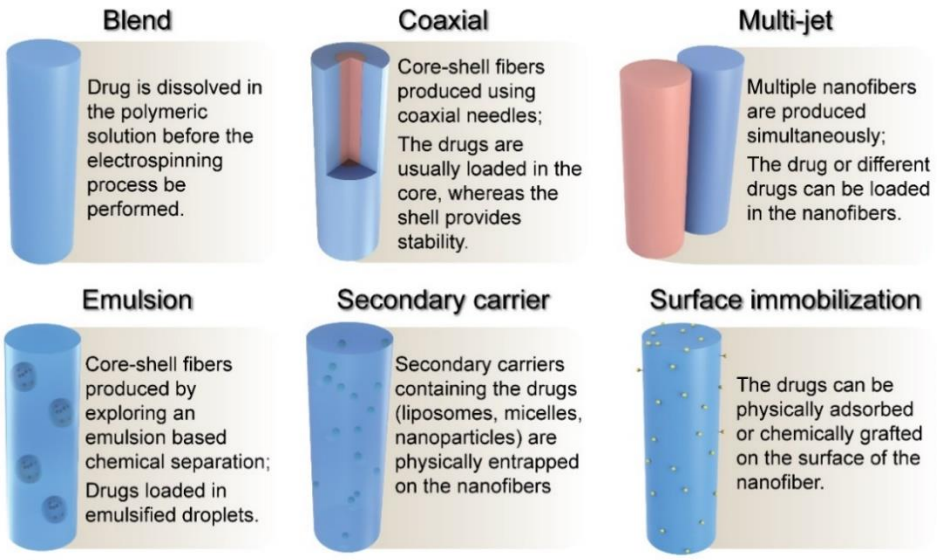

Figure 9. Illustration of the main strategies used to incorporate drugs into electrospun nanofibers (reproduced from [93]).

By combining these strategies, researchers can control the encapsulation of multiple biomolecules. Depending on the role of a biomolecule in the healing process, the drug release profile can be tailored through the incorporation method used [94]. For example, the physical adsorption of biomolecules into nanofibers is frequently associated with burst releases and short diffusion times, whereas the co-axial electrospinning allows a more controlled and sustained release profile [95, 96]. On the other hand, if the different molecules are incorporated into nanofibers by the same method, the drug release profile will be dependent on the diffusion coefficient of each molecule. In these cases, the rate of biomolecule diffusion out of the polymeric matrix will be affected by several factors like polymer swelling, polymer erosion, biomolecular dissolution/diffusion characteristics, biomolecules distribution inside the matrix and biomolecule/polymer ratio [97-99].

Considering all these properties, researchers have been incorporating different antibacterial and biological agents into nanofibers to improve their performance in the healing process [100, 101]. The results obtained revealed that these dressings are able to avoid bacterial penetration (*e.g.* nanofibers functionalized with antibiotics, silver-based materials, and bactericidal natural compounds) or to enhance the wound healing (*e.g.* nanofibers incorporating GFs, vitamins, and anti-inflammatory molecules) [25, 102-104].

1.4.3.1. Ibuprofen

Ibuprofen (IBP) is a non-steroidal anti-inflammatory (NSAID), antipyretic and pain relief molecule. IBP inhibits two isoforms of cyclooxygenase (COX-1 and COX-2) enzymes that are responsible for prostaglandin biosynthesis [103, 105]. The chemical structure of IBP is presented in Figure 10. The anti-inflammatory behavior of IBP has been particularly assessed in osteoarticular, venous legs ulcers, and muscle healing by oral administration [106, 107].
In the treatment of the skin injuries, the use of anti-inflammatory molecules is crucial in cases where an extended and prolonged inflammation occurs. The continuous attraction of neutrophils and macrophages leads to the excessive production of inflammatory mediators, free radicals, and cytotoxic enzymes, which interrupt the physiological healing mechanisms and induction damage to the surrounding tissue [62, 108, 109].
Considering this, the researchers have been incorporating anti-inflammatory molecules into wound dressing for avoiding the development of a chronic inflammation and accumulation of free radicals. So, Mohiti-Asli and colleagues incorporated IBP (20%) into PLA nanofibers to promote the regeneration of full thickness wounds. These researchers noticed that this membrane supported cell adhesion and proliferation, while *in vivo* assays demonstrated their ability to promote the wound closure (60% wound contraction after 14 days) [110].

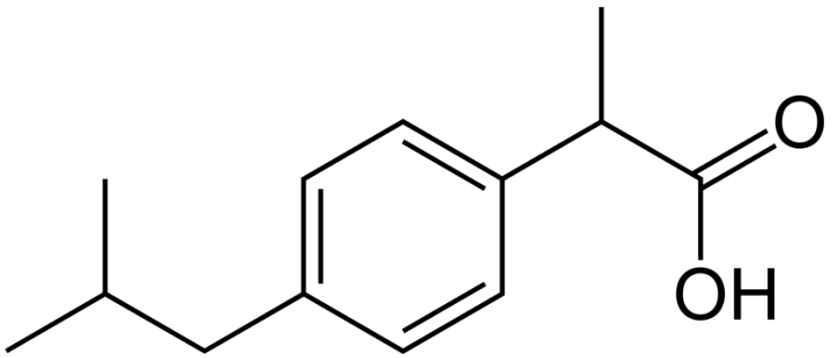

Figure 10. Representation of chemical structure of IBP.

1.4.3.2. Lavender oil

The antibacterial activity of wound dressings is another crucial feature, since the invasion of the wound site by microorganisms will promote the destruction of the granulation tissue, GFs and ECM components, impairing the healing process [111, 112]. In this way, the researchers have been incorporating different types of the antimicrobial molecules *(e.g.* antibiotics, silver nanoparticles and natural extracts-derived products) into the wound dressings. However, the continued administration of antibiotics promoted the appearance of the multidrug resistant bacteria, while the metallic nanoparticles can present toxic effects for skin tissue [113]. Such facts have propelled the researchers to study other antimicrobial molecules such as plant extracts and essential oils (EOs) [114-118]. Lavender oil (LO) is an EO, which is obtained through

extraction from lavender plant species such as *Lavandula latifolia*, *Lavandula stoechas*, *Lavandula x intermedia* and *Lavandula angustifolia* [119].

The LO is manly composed of terpenes (≈ 64%, linalool (its chemical structure is represented in Figure 11), linalyl acetate, 1,8-cineole, ß-ocimene, terpinen-4-ol), and ketones (≈ 13%, as camphor), which confers it antimicrobial activity [120, 121]. The antibacterial mechanism of LO is attributed to their hydrophobic character and their components promote the partition of the lipids present in the cell membrane, increasing their permeability, and consequently, leading to the bacterial cells death due to the leakage of essential molecules and ions [118, 122, 123]. Additionally, the LO also possesses antifungal, antioxidant, analgesic and anti-inflammatory activity [124, 125].

In tissue engineering applications, there are some works that reported the incorporation of LO into nanofibers. For example, Balasubramanian *et al*. incorporated LO into polyacrylonitrile electrospun nanofibers, by using the blend electrospinning technique. These authors verified a clear zone of inhibition with a diameter of 14-15 mm against *Staphylococcus aureus* (*S.aureus*) and *Klebsiella pneunoniae* after 8 h of incubation, which remained unaltered for more 30 days [126]. Another study, Hajiali and colleagues produced sodium alginate nanofibrous incorporating LO, through blend electrospinning. The authors noticed that the nanofibers incorporated with LO exhibited a high antibacterial efficacy, they showed an average inhibition diameter of 21.7 ± 1.6 mm against *S.aureus* [108].

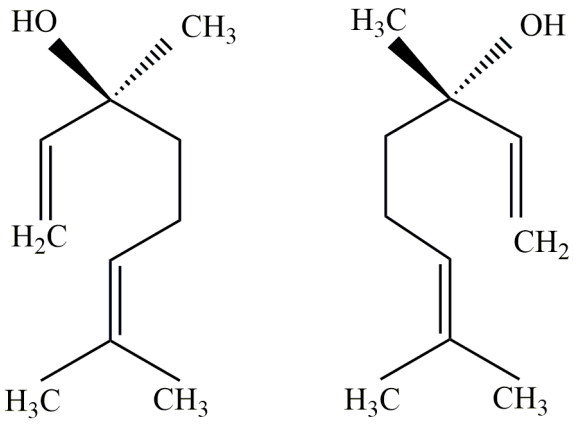

Figure 11. Representation of chemical structure of main component of LO (Linalool).

1.5. Aims

The overall aim of the present Master dissertation work plan was to produce and characterize a new electrospun membrane to be used as drug delivery system during the wound healing process (Figure 12). Molecules displaying anti-inflammatory (IBP) and antibacterial (LO) properties were incorporated into nanofibers, through different methods aiming to obtain distinct drug release profiles, in order to fulfill the demands of the specific phases of wound healing process.

The specific objectives of this study were:

- Optimize and produce PVA_Lys membrane;
- Incorporate an anti-inflammatory molecule (IBP) into nanofibers through blend electrospinning, resulting in the PVA_Lys_IBP membrane;
- Incorporate an antibacterial molecule (LO) on the surface of the membrane, by physical adsorption method, yielding to PVA_Lys_LO membrane;
- Evaluate and characterize the physicochemical properties of the produced membranes;
- Evaluate and characterize the drug release profile of IBP and LO from PVA_Lys_IBP and PVA_Lys_LO membranes, respectively;
- Evaluate and characterize the biological properties of the produced membranes;
- Evaluate and characterize the antioxidant and antimicrobial properties of the produced membranes.

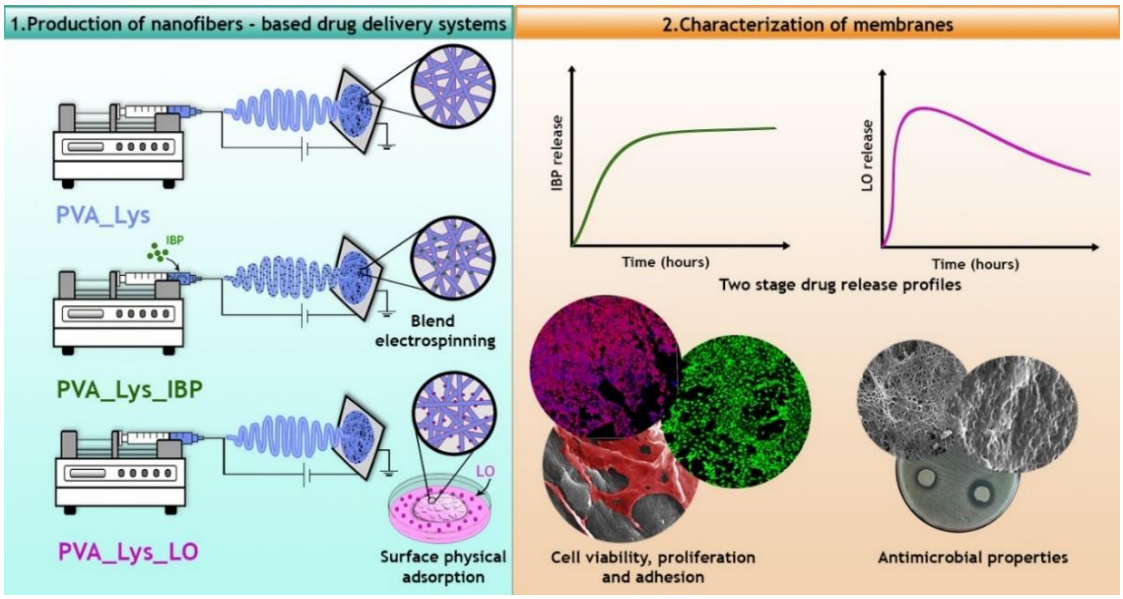

Figure 12. Schematic representation of the experimental setup used herein to produce the electrospun membranes-based drug delivery systems. The PVA_Lys membrane was obtained through the combination of PVA and Lys; PVA_LYS_IBP membrane was achieved by dissolving the IBP in the PVA and Lys solution, followed by their use in the electrospinning process; PVA_Lys_LO membrane was obtained by the surface physical adsorption of LO at membrane' surface. After the production of the membranes, their morphological, physicochemical, mechanical and biological properties were evaluated.

Chapter II - Materials and Methods

2. Materials and Methods

2.1. Materials

Fetal bovine serum (FBS) free from any antibiotic was purchased from Biochrom AG (Berlin, Germany). Normal human dermal fibroblasts (NHDF) cells were acquired from PromoCell (Labclinics, S.A., Barcelona, Spain). 3-(4,5-dimethylthiazol- 2-yl)-5-(3-carboxymethoxyphenyl)-2 (4-sulfophenyl)-2H-tetrazolium (MTS) was bought from Promega (Madison, WI, USA). L-lysine (98%, Mw =146,19 g/mol) was obtained by Acros organics (China). Ibuprofen (IBP) was bought by TCI (Tokyo Chemical Industry). Lavender oil (LO) was acquired by Keypharm (Belgium). Dulbecco's modified eagle's medium (DMEM-F12), Poly(ethylene oxide) (Mw=300,000 g/mol), Poly(vinyl alcohol) (Mw=89,000-98,000 g/mol) 99% hydrolyzed, ethylenediaminetetraacetic acid (EDTA), glutaraldehyde, LB Broth, phosphate-buffered saline solution (PBS), 2,2-diphenly-1-picrylhydrazyl (DPPH), TritonX-100 and trypsin were purchased from Sigma-Aldrich (Sintra, Portugal). Quant-iT Pico Green dsDNA assay kit and Hoechst 33342® were obtained from ThermoFisher Scientific (Waltham, MA, USA). *Staphylococcus aureus* clinical isolate (*S.aureus*) ATCC 25923 and *Pseudomonas aeruginosa* (*P.aeruginosa*) obtained from a human sample, were used as models of prokaryotic organisms to evaluate the bactericidal activity exhibited by the produced membranes. Propidium iodide buffer and WGA-Alexa 594® conjugate were gotten from Invitrogen (Carlsbad, California, EUA) and Calcein AM was supplied by Calbiochem (Merck Millipore, Oeiras, Portugal). A Milli-Q Advantage A10 ultrapure Water Purification System (0.22 μm filtered; 18.2 MΩ/cm at 25 °C) was used to obtained double deionized and filtered water.

2.2. Methods

2.2.1. Production of electrospun membranes

The electrospun membranes were produced by using a conventional electrospinning apparatus. This equipment was composed by a high voltage source (Spellman CZE1000R, 0–30 kV), a precision syringe pump (KDS-100), a plastic syringe with a stainless-steel needle (21 Gauge), and an aluminum foil connected to a copper collector.

Initially, a PVA solution 9% (w/v) was dissolved in Milli-Q water at 90 ºC, under stirring, for 1h. Subsequently, the temperature was reduced to 60°C and then the L-lysine, at a concentration of 12.5 mg/mL, was added to the solution, and mixed under magnetic stirring for 30 min. Lastly, 2 mL of PEO solution (8% w/v) were added to obtain a solution with a viscosity that is suitable for the electrospinning process be performed. After that, 10 mL of the solution were placed in the syringe, and electrospun using a constant flow rate (1 mL/h), a working distance of 12 cm, and an applied voltage of 30 kV, leading to the production of a **PVA_Lys** membrane.

In turn, the **PVA_Lys_IBP** membrane was obtained through the addition of IBP (at 1 mg/mL) to the PVA_Lys solution, before the electrospinning process be performed. On the other side, the LO was adsorbed at surface of the PVA_Lys membrane by exploring the electrostatic interactions that occur between the positively charged amine groups of Lys and the electronegative groups (*e.g.* acetate, aldehyde, and terpenoid moieties) found in LO. For that purpose, 15 µL of LO (at a concentration of 1.3 mg/mL) were placed at the PVA_Lys membrane' surface (0.79 cm^2) and incubated at 50 ºC, under vacuum, during 1 h, yielding to **PVA_Lys_LO** membrane.

2.2.2. Characterization of the membranes' morphology

The produced membranes were analysed to Scanning electron microscopy (SEM) to characterize their morphology and the fibers diameter. To accomplish that, the samples were assembled onto aluminum stubs using Araldite glue, and sputter-coated with gold using a Quorum Q150R ES sputter coater (Quorum Technologies Ltd., Laughton, East Sussex, UK). The SEM images were obtained using the Hitachi S-3400 N Scanning Electron Microscope (Hitachi, Tokyo, Japan), at an accelerating voltage of 20 kV. The nanofibers' diameter was measured using an image analysis software – Image J (Scion Corp., Frederick, MD) [127].

2.2.3. Attenuated total reflectance-Fourier transform infrared spectroscopy analysis

To characterize the chemical composition of the membranes, attenuated total reflectance-Fourier transform infrared spectroscopy (ATR-FTIR) analysis was used. The membranes' spectra were obtained with an average of 128 scans, a spectral width ranging from 4000 and 400 cm^{-1} and a spectral resolution of 32 cm^{-1}, using a Nicolet iS10 FTIR spectrophotometer (Thermo Scientific, Waltham, MA, USA). In addition, the raw materials used for membranes production were also subjected to spectral analysis for comparative purposes.

2.2.4. Characterization of the mechanical properties of the membranes

The mechanical properties of the electrospun membranes were evaluated using a Shimadzu AG-X Tensile Testing Machine (Tokyo, Japan), at room temperature (RT), under wet and dry conditions, accordingly to the guidelines established by the Standard Test Method for Tensile Properties of Polymer Matrix Composite Materials (ASTM standard D3039/ D3039 M) [107].

To perform this assay, samples (n = 5) with a width of 2 cm, gauge length of 6 cm and thickness ranging from 0.41 to 0.52 mm were used. The length between the clamps was set to 2 cm and the speed of testing was set to 20 mm/min. For the wet conditions, the membranes were previously immersed in a PBS solution (pH 5.5), over 24 h, at 37 ºC. Load-extension data was

recorded and the stress–strain curve of the membranes was obtained through Equations (1) and (2), respectively:

$$Stress = \sigma = \frac{F}{A} \qquad (1)$$

$$Strain = \frac{\Delta l}{L} \qquad (2)$$

where F is the applied force; A is the cross-sectional area; Δl is the change in length; and L is the length between the clamps.

2.2.5. Evaluation of the membranes' porosity

The total porosity of the membranes was evaluated by using a liquid displacement method described elsewhere [69]. For this assay, five specimens were weighed and then immersed in absolute EtOH during 1h. Then, the samples were re-weighted, and the membranes' overall porosity was determined through Equation (3):

$$Porosity\ (\%) = \frac{W_s - W_d}{D_{ethanol} \times V_{membrane}} \times 100 \qquad (3)$$

where W_s and W_d represent the swollen and dry weights of the membrane, respectively. The $D_{ethanol}$ is the density of the ethanol at RT, and $V_{membrane}$ is the volume of the swollen membrane.

2.2.6. Evaluation of membranes' wettability

The wettability of the membranes was characterized by determining the water contact angle (WCA) at their surfaces. To accomplish that, the WCA was measured using the Data Physics Contact Angle System OCAH 200 apparatus, operating in static mode, at RT [77]. This assay consisted on the deposition of water drops (4 μL) at different locations of the electrospun membranes' surface.

2.2.7. Water vapor transmission rate (WVTR)

The water vapor diffusion through the membranes was determined as reported elsewhere [128]. Briefly, the membranes were used to seal the opening of a glass test tube (1.77 cm^2) containing 10 mL of ultrapure water. To prevent non-specific water evaporation, parafilm tape was used to fix the membrane in glass tube. Posteriorly, the membranes were incubated at 37 ºC and the amount of evaporated water was measured by monitoring the weight variations at specific time points. Then, the WVTR was obtained through Equation (4):

$$\text{Water Vapor Transmission Rate} = \frac{W_{loss}}{A} \qquad (4)$$

where W_{loss} is the daily weight loss of water and A is the area of the tube opening.

2.2.8. Evaluation of the swelling capacity of the produced membranes

The swelling capacity of the produced membranes was determined by immersing them in a PBS solution at pH 5 (pH of native skin) or pH 8 (pH found in a skin injury), at 37 ºC, under stirring (40 rpm) [77]. After, the excess of PBS be removed with a filter paper, the samples were weighted. In turn, the swelling ratio was calculated using Equation (5):

$$Swelling\ ratio\ (Q) = \frac{W_t}{W_0} \qquad (5)$$

where W_t is the final weight and W_0 is the initial weight of the membranes.

2.2.9. Characterization of the biodegradation profile of the membranes

The degradation profile of the membranes was monitored by immersing the samples in PBS, under stirring (40 rpm), at 37 ºC. After 1, 3 and 7 days, the membranes were removed from the solutions, fully dried and weighed. Then, the degradation percentage was calculated at each time through Equation (6):

$$Weight\ loss\ (\%) = \frac{W_i - W_t}{W_t} \times 100 \qquad (6)$$

where W_i corresponds to the initial weight of the sample and W_t to the weight of the sample at time t.

2.2.10. Evaluation of antioxidant capacity of the membranes

The antioxidant activity of the membranes was evaluated through the 2-diphenly-1-picrylhydrazyl (DPPH) radical scavenging assay, as previously described in the literature [77, 127]. To perform this assay, membrane samples (5 mg) were immersed in 3 mL of DPPH solution (100 µM) in methanol and incubated in a dark room, at RT, during 30 min. Afterwards, the absorbance of each mixture was recorded using a microplate reader (Biorad xMark microplate spectrophotometer), at 517 nm. The antioxidant activity was then calculated using the Equation (7):

$$Antioxidant\ activity\ (\%) = \frac{A_c - A_s}{A_c} \times 100 \qquad (7)$$

where A_c and A_s represent the control and sample absorbance values, respectively.

2.2.11. Evaluation of the encapsulation and loading efficiency of IBP and LO within membranes

The method used to study the IBP and LO encapsulation and loading efficiencies was adapted from Miguel *et al*. [77]. The PVA_Lys_IBP and PVA_Lys_LO membranes were subjected to a total degradation, through their immersion in hot water, under sonication during 2h. Then, the samples were centrifuged at 18 000 *g*, for 10 min. The supernatant absorbance was recorded using a Thermo Scientific Evolution 201 UV-vis spectrophotometer, at 264 and 223 nm, for IBP and LO, respectively. After that, the IBP and LO concentrations were determined using standard calibration curves for IBP (y = 1.4263x + 0.0196, R^2= 0.999) and for LO (y = 1.3833x + 2.6952, R^2= 0.996). The encapsulation efficiency (EE) and loading efficiency (LE) for both bioactive molecules were determined using the Equations 8 and 9 [129]:

$$EE(\%) = \frac{W_i - W_s}{W_i} \times 100 \qquad (8)$$

$$LE(\%) = \frac{W_i - W_s}{Y} \times 100 \qquad (9)$$

where W_i is the total amount of biomolecule (IBP or LO) added for loading, W_s is the amount of molecule present in the supernatant, and Y is the total dry weight of PVA_Lys_IBP and PVA_Lys_LO membranes.

2.2.12. *In vitro* IBP and LO release profile and analysis of the drug-release kinetics

The amount of IBP and LO released at two pHs values (pH 5 and pH 8) was determined following the protocols already described in the literature [77, 107, 126]. Briefly, the PVA_Lys_IBP and PVA_Lys_LO membranes (15 mg) were incubated at 37 ºC, under stirring (40 rpm), with 1 mL of PBS at pH 5 or 8. Then, at specific timepoints, the samples were centrifugated at 18000 *g*, for 10 min, and the supernatant' absorbance was measured.

Moreover, the IBP and LO drug release kinetics were characterized by using Peppas-Korsmeyer (10), Higuchi (11), and first order (12) models.

Peppas-Korsmeyer: $\frac{M_t}{M_\infty} = \mathrm{Kt^n}$ *(10)*

Higuchi: $Q_t = K_H t^{1/2}$ *(11)*

First-order: $Ln\ Q_t = Ln\ Q_0 + K_1 t$ *(12)*

where M_t is the cumulative amount of drug released at time t, M_∞ is the initial drug loading, K is a constant characteristic of the drug-polymer system, and n is the diffusion exponent, explaining the nature of the release mechanism. Q_t is the amount of drug dissolved in time t, Q_0 is the initial amount of drug in the solution, K_H is the Higuchi dissolution constant and K_1 is the first-order release constant.

2.2.13. Characterization of the biological properties of the produced membranes

2.2.13.1. Evaluation of cell viability and proliferation in contact with electrospun membranes

The membranes' biocompatibility was characterized through an MTS assay, according to the ISO 10993-5:2009 (Biological evaluation of medical devices - Part 5: Tests for *in vitro* cytotoxicity). To perform this assay, samples with sizes inferior to 10% of the well area, were placed into 96-well plates, and then sterilized under UV irradiation (254 nm, ≈ 7 mW cm^{-2}) during 1h. Then, NHDF cells were seeded at a density of 10×10^3 cells per well and incubated at 37 °C, in an incubator with a 5% CO_2 humidified atmosphere. After 1, 3 and 7 days of incubation, the medium of each well was removed and replaced by a mixture of 100 µL of fresh culture medium and 20 µL of MTS/PMS (phenazine methosulfate) reagent solution. Following 4h of incubation (at 37 °C, in a 5% CO_2 atmosphere), the samples absorbance was measured at 490 nm using a microplate reader (Biorad xMark microplate spectrophotometer). Further, the positive control (K^+) and negative control (K^-) were also used, which correspond to the cells incubated with ethanol (70%) and cells incubated only with culture medium, respectively.

2.2.13.2. dsDNA quantification

The NHDF proliferation in the presence of the membranes was evaluated by measuring the dsDNA content using a Quant-iT PicoGreen dsDNA Assay kit, as reported in the literature [69, 77, 127]. Initially, the cells were placed in contact with the produced membranes. After 1, 3 and 7 days of incubation, the cell lysis was induced by adding Triton X-100 (1×) on the wells during 1h. Then, the membranes were transferred into a 1.5 mL Eppendorfs and subjected to a freeze-thaw cycle. Posteriorly, the samples were sonicated and centrifuged 18000 *g* for 15 min and the supernatant was collected. After, 100 µL of supernatant was added to an equal volume of PicoGreen solution in TE buffer (1×). Lastly, the plate was incubated in the dark during 10-15 min and the fluorescence was measured at excitation and emission wavelengths of 485 nm and 535 nm using a microplate reader. To quantify the dsDNA concentrations, a calibration curve was performed using samples with known concentrations of dsDNA.

2.2.13.3. Live/Dead assay

The presence of viable and dead cells on the produced membranes was monitored by using the Live/dead assay. For that purpose, cells (10 × 10^3 cells/mL) were seeded in contact with membranes in µ-Slide 8 well Ibidi imaging plates (Ibidi GmbH, Germany). Cells seeded with only culture medium were used as negative control (K^-), while those treated with Triton X-100 were used as positive control (K^+). After 1, 3 and 7 days, samples were stained with Calcein (2 µM) and Propidium iodide (15 mM), following the instructions of the manufacturer. Then samples were imaged with a confocal laser scanning microscope (CLSM, Zeiss, Oberkochen, Germany) and processed in the Zeiss Zen 2010 software (Zeiss, Oberkochen, Germany).

2.2.13.4. Characterization of cell proliferation through confocal microscopy analysis

The cell distribution and proliferation at the electrospun membranes' surface was evaluated by CLSM. To perform that, cells (10 x 10^3 cells/mL) were seeded in µ-Slide 8 well Ibidi imaging plates (Ibidi GmbH, Germany) in contact with membranes. After 1 and 3 days of incubation, the cells were stained with the WGA-Alexa 594® conjugate (5 µM) and Hoechst 33342® (2 µM), to label the cytoplasm (red) and cell nucleus (blue), respectively. The 3D reconstruction and the image analysis were performed using Zeiss Zen 2010 software (Zeiss, Oberkochen, Germany).

2.2.14. Evaluation of the antimicrobial properties of the produced membranes

Membranes' antimicrobial activity was studied through the determination of the inhibition area produced by the membranes when in contact with *S.aureus* or *P.aeruginosa*. Briefly, 200 µL of bacteria medium containing 1 × 10^8 CFU/mL of *S.aureus* or *P.aeruginosa* were inoculated in LB agar plates. Then, circular samples of the membranes (1 cm of diameter) were placed in the plate and then incubated for 24h, at 37°C.

The percentage of inhibition area was calculated using Equation (13):

$$Inhibition\ area\ (\%) = \frac{A_i - A_0}{A_i} \qquad (13)$$

where, A_i and A_0 represent the inhibition area and the area of the membranes' disc, respectively.

In addition, the antibacterial effect of the membranes against *S.aureus* and *P.aeruginosa* was also evaluated by quantifying the colony forming units. Briefly, 50 mg of each membrane sample was added to 10 mL of LB broth containing 1 × 10^5 CFU/mL of early mid-log phase bacteria

culture and then incubated at 37 °C, for 24 h. After the incubation period, serial dilutions were prepared and 100 µL of bacterial samples were transferred into LB agar plates and incubated for 24 h, at 37 °C. The bacterial colonies were then counted and defined as CFU/mL. The antibacterial efficiency of the membranes was calculated through Equation (14):

$$Antibacterial\ efficiency\ (\%) = \frac{N_0 - N}{N} \times 100 \quad \textit{(14)}$$

where N_0 and N represents the CFU/mL of control and experimental group, respectively.

2.2.15. Characterization of biological properties of the membranes through SEM analysis

The cellular adhesion and biofilm formation at the PVA_Lys, PVA_Lys_IBP and PVA_Lys_LO membranes' surface was characterized through SEM analysis. Initially, samples containing cells or bacteria were fixed with 2.5% (v/v) glutaraldehyde for 15 min and 30 min, respectively. Following this, samples were frozen during 1-2 h and freeze-dried for 3 h (for samples containing cells) and 6 h (for samples with bacteria). Lastly, the samples were prepared for SEM analysis, according to the protocol previously described in section 2.2.2.

2.2.16. Statistical Analysis

The statistical analysis of the obtained results was performed using one-way analysis of variance (ANOVA), with the Newman-Keuls post hoc test. A p value lower than 0.05 ($p<0.05$) was considered statistically significant.

Chapter III - Results and Discussion

3. Results and discussion

3.1. Characterization of the morphological and physicochemical properties of produced nanofibrous membranes

The advances in the area of nanotechnology highlighted the promising properties of the electrospun nanofibers to act as a drug delivery systems [93, 130]. Indeed, the application of the nanofibrous carriers allows a site-specific release of the drugs, reducing the total amount of drug dose required to exert the therapeutic effect as well as minimize the nontargeted site toxicities [97]. Herein, a PVA_Lys electrospun membrane-based drug delivery system was produced, in which IBP or LO were incorporated, by using blend electrospinning and surface physical adsorption, respectively. The morphological properties of the produced membranes were investigated through SEM analysis, and the fibers' diameter was assessed by performing SEM images analysis with ImageJ software (as seen in Figure 13). The results showed that the electrospun membranes displayed a randomly oriented mesh composed of highly interconnected fibers with bead-free smooth surface. Moreover, the PVA_Lys, PVA_Lys_IBP, and PVA_Lys_LO fibers had a mean diameter value of 474.22 ± 144.85 nm, 385.03 ± 108.21 nm and 487.14 ± 155.81 nm, respectively. Such results show that the incorporation of IBP promotes a decrease on the fibers diameter when compared with PVA_Lys membrane, while the LO inclusion did not induce any noticeable changes on the fibers size. Such differences may be related to the method used for the biomolecules loading (blend or surface adsorption), the establishment of hydrophobic interactions between the IBP and the PVA_Lys, or the decrease on electrospinning solution surface tension mediated by IBP incorporation [131]. Similar results were previously obtained by Pires *et al*. who reported a decrease in the poly(trimethylene carbonate-co-ε-caprolactone) nanofibers diameter from 1.09 ± 0.10 μm (for non-loaded fibers) to 0.84 ± 0.08 μm (for fibers loaded with IBP 5%) [132]. In a similar way, Liu *et al*. also noticed that the mean fiber diameter decreased by raising the IBP concentration, *i.e*. 1.45 ± 0.71 mm (without IBP), 1.40 ± 0.52 mm (2% IBP), 1.32 ± 0.67 mm (6% IBP) and 1.25 ± 0.59 mm (10% IBP) [133].

On the other side, the incorporation of LO into PVA_Lys nanofibers through the surface physical adsorption technique allowed the production of the PVA_Lys_LO membrane displaying a more irregular and rougher surface. Such methodology has been frequently used to immobilize growth factors and heparin at the nanofibers' surface without inducing significant differences on the nanofibers morphology [134]. Additionally, it is worth to notice that all the electrospun membranes presented nanofibers diameters that are within the range of collagen fibrils found at the ECM (50-500 nm), increasing its structural similarity with the native skin tissue [25, 69, 76].

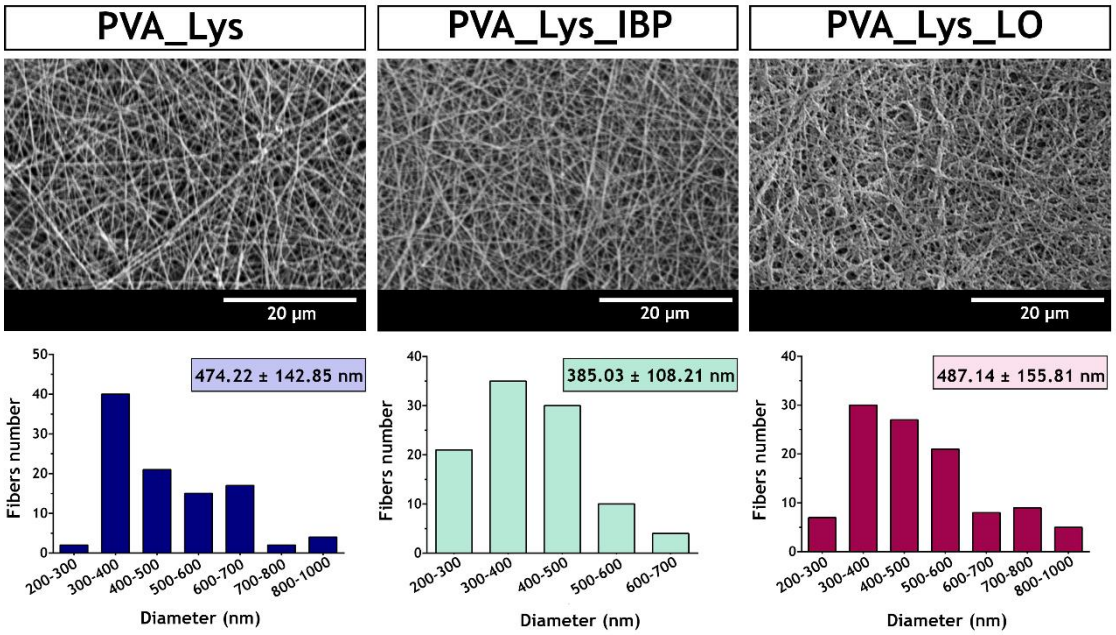

Figure 13. Characterization of the electrospun membranes (PVA_Lys, PVA_Lys_IBP and PVA_Lys_LO) morphological features. SEM images and analysis of the respective nanofibers' diameter distribution.

Furthermore, the chemical composition of the membranes was assessed through ATR-FTIR analysis. The spectra of raw materials used for membranes' production are presented in Figure 14A. The PVA spectrum presents its characteristics peaks at 3299 cm^{-1} (O-H stretching), 2917 cm^{-1} (asymmetric CH_2 stretching), 1427 cm^{-1} (CH-O-H stretching), 1085 cm^{-1} (C-O stretching), and 838 cm^{-1} (C-C stretching) [73, 135]. In turn, the Lys amide (I) and amide (II) vibrations are clearly visible at 1572 and 1511 cm^{-1}, respectively [80, 136]. Further, it is also possible to observe the characteristic band (CH_2) of PEO in the region between 2900 cm^{-1} and 2850 cm^{-1} [69]. On the other side, Figure 14B displays the characteristics peaks of the biomolecules incorporated into PVA_Lys membranes. The spectrum of IBP evidenced its two characteristic peaks: at 2941 cm^{-1} (OH bending) and at 1703 cm^{-1} (C=O stretching) [137, 138]. In turn, in the LO spectrum presents a broad peak at 3457 cm^{-1} (O-H stretch, demonstrating the presence of alcohol); at 2963 cm^{-1} (C=C), 2924 cm^{-1} (stretching of methyl groups); strong bands at 1732 cm^{-1} (C=O), 1371 cm^{-1} and 1246 cm^{-1} (C-O) of ester groups. In addition, it is possible to also observe in this spectrum the peaks at 1008 cm^{-1}, 919 cm^{-1}, 833 cm^{-1} and 609 cm^{-1}, which belong to LO C-H deformations [126, 139].

Through the analysis of the spectra of the membranes (Figure 14B), it is noticeable the presence of the characteristic peaks of its raw materials (PVA, Lys, PEO). Furthermore, the peaks of IBP and LO can also be observed in the spectrum of PVA_Lys_IBP and PVA_Lys_LO membranes, respectively, indicating the successful loading of the biomolecules within the PVA_Lys polymeric nanofibers.

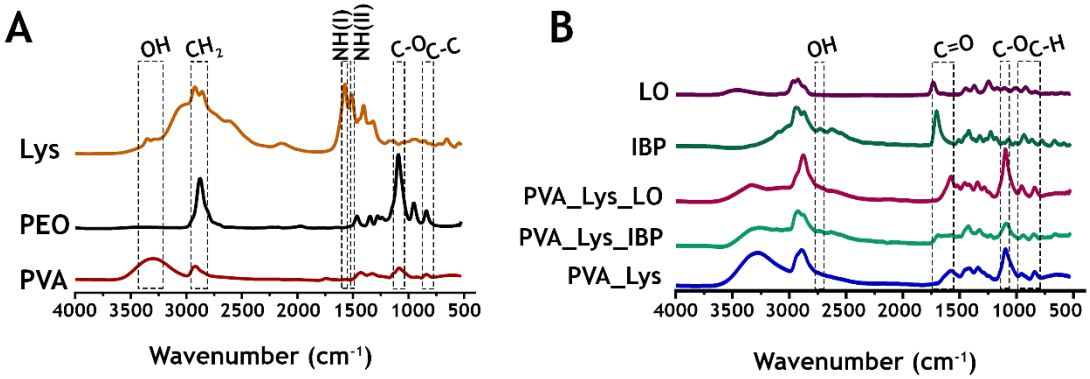

Figure 14. ATR-FTIR analysis of the raw materials (A) and raw biomolecules (IBP and LO) and the produced electrospun membranes (B).

3.2. Characterization of the membranes' mechanical properties

The mechanical properties of the PVA_Lys, PVA_Lys_IBP and PVA_Lys_LO membranes were determined in dry and wet conditions [69]. The Young's modulus, tensile strength, and elongation at break of the membranes and the values displayed by native skin are presented in Table 3. The Young's modulus obtained for PVA_Lys, PVA_Lys_IBP, and PVA_Lys_LO membranes in dry state were 74.67 ± 10.00 MPa, 72.75 ± 14.73 MPa, and 44.95 ± 10.52 MPa, respectively. Nevertheless, these values decreased when the membranes were tested in wet conditions, 0.73 ± 0.25 MPa, 0.88 ± 0.35 MPa, and 1.43 ± 0.85 MPa for PVA_Lys, PVA_Lys_IBP, and PVA_Lys_LO membranes, respectively. Further, the PVA_Lys, PVA_Lys_IBP, and PVA_Lys_LO membranes showed values of Tensile Strength of 4.53 ± 1.02 MPa, 2.78 ± 0.66 MPa, and 2.89 ± 1.94 MPa in dry state, and 1.57 ± 2.92 MPa, 0.87 ± 1.45 MPa and 0.54 ± 0.04 MPa in wet conditions, respectively. On the other side, the PVA_Lys, PVA_Lys_IBP, and PVA_Lys_LO membranes can bear a strain of 8.18 ± 5.23%, 4.62 ± 0.27%, and 8.75 ± 6.21% for the dry state and 13.09 ± 5.55%, 18.15 ± 1.17%, and 20.17 ± 3.55% for the wet state, respectively.

The obtained results demonstrate that the drug incorporation methodologies did not impact on the membranes' mechanical behaviour. In fact, all the test groups presented similar mechanical properties (Young's modulus, tensile strength, and elongation at break). Further, in dry state, the mechanical parameters of the membranes are close to those exhibited by the native skin (Table 3) [107]. On the other side, the assays conducted under wet conditions reveal a decrease in both the Young modulus and tensile strength for all the tested samples. Such reduction on the membranes' mechanical performance under wet conditions can be attributed to the highly hydrophilic character of the membranes' raw materials (PVA and Lys) [85]. These will facilitate the membranes interaction with the water molecules, that will have impact on their swelling profile as well as on the intermolecular forces established between the polymeric chains, leading to an increased molecular mobility [140]. Similar results were also observed for CS/PEO

electrospun membranes produced by An *et al.* [138], and for CS electrospun membranes fabricated by Li *et al.* [141].

Overall, the obtained results demonstrate the suitability of the produced membranes to provide adequate mechanical support during the tissue remodelling process as well as the capacity to endure all the mechanical stresses that membranes suffer during its handling.

Table 3. Mechanical properties exhibited by the produced membranes. Data are presented as the mean ± standard deviation (n = 5). The reference values for the native human skin were obtained from [107].

		Young Modulus (MPa)	Tensile Strength (MPa)	Elongation at break (%)
PVA_Lys	Dry	74.67 ± 10.00	4.53 ± 1.02	8.18 ± 5.23
	Wet	0.73 ± 0.25	1.57 ± 2.92	13.09 ± 5.55
PVA_Lys_IBP	Dry	72.75 ± 14.73	2.78 ± 0.66	4.62 ± 0.27
	Wet	0.88 ± 0.35	0.87 ± 1.45	18.15 ± 1.17
PVA_Lys_LO	Dry	44.95 ± 10.52	2.89 ± 1.94	8.75 ± 6.21
	Wet	1.43 ± 0.85	0.54 ± 0.04	20.17 ± 3.55
Native skin		4.6-20	5-30	35-115

3.3. Determination of the total porosity of the membranes

For skin regenerative purposes, the membranes' porosity determines their capacity to promote the exudate absorption, cell accommodation, nutrients and gas exchanges, and waste excretion [142]. According to the literature, a wound dressing must present an overall porosity within the range of 60-90% for an effective healing process to occur [77, 143]. Herein, the produced membranes presented a total porosity value of 69.29 ± 1.54%, 77.70 ± 14.13% and 54.15 ± 3.24% for PVA_Lys, PVA_Lys_IBP, and PVA_Lys_LO membranes, respectively (Figure 15A). The obtained results revealed that the incorporation of IBP did not affect the total porosity of the membranes, whereas the LO adsorption at surface of nanofibers promoted a decrease on their total porosity. Such differences are also corroborated by the structural alterations observed in the SEM images (Figure 13). Indeed, the nanofibers of PVA_Lys_LO membranes exhibit fibers with higher mean diameters, increased surface roughness, and lower number of void spaces. Such morphological alterations have been related to a decrease on the membranes porosity [144]. Nonetheless, all the produced membranes exhibited porosity values within the range considered as ideal to provide the required space for cellular accommodation, migration, nutrient exchange and production of new ECM.

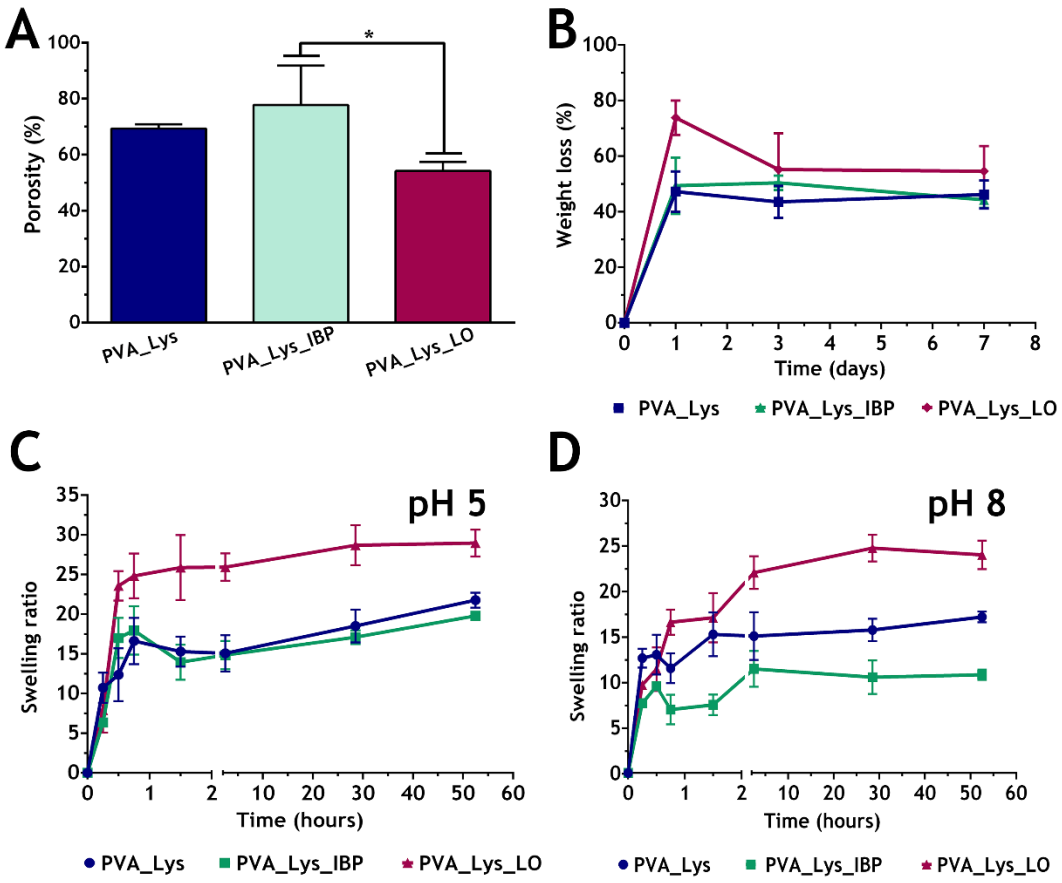

Figure 15. Characterization of the porosity (A), weight loss (B) and swelling profile at pH 5 (C) and at pH 8 (D) of the PVA_Lys, PVA_Lys_IBP and PVA_Lys_LO membranes. Data are presented as the mean ± standard deviation, n = 5, *p< 0.05).

3.4. Evaluation of the weight loss of the membranes

Traditional wound dressings need to be removed from the wound site, in a process that can induce further lesions, increase the formation of scar tissue, as well as, facilitate the wound bacterial contamination [145]. In this way, tissue engineering researchers have been focused on the development of biodegradable wound dressings that present a degradation profile similar to the rate of new tissue formation. Herein, the weight loss of the different membranes was evaluated along 7 days of incubation (Figure 15B). The results highlight a more pronounced weight loss at day 1 for PVA_Lys_LO membranes (73.79 ± 6.18%) in comparison with the PVA_Lys (47.20 ± 7.27%) and PVA_Lys_IBP (49.53 ± 10.12%). Such difference can be attributed to the dissociation of the LO weak electrostatic interactions (occurring between the negatively charged acetate, aldehyde, and terpenoid groups of LO and amine groups of Lys) with the surface of the PVA_Lys membrane and consequent drug release [146-148].

On the other side, the weight loss profile exhibited after 3 and 7 days of incubation is similar among the different membranes. Such degradation profile of the membranes in a non-enzymatic solution is justified by the hydrolysis of the PVA and Lys when incubated at 37 °C in PBS [73, 149].

3.5. Characterization of electrospun membranes' swelling profile

During the healing process, the majority of the exudate is produced during the inflammatory phase. The excessive accumulation of wound exudate can induce the tissue maceration, and facilitate the occurrence of infections [150]. Therefore, the wound dressings must be able to avoid the excessive accumulation of exudates as well as maintain a moist environment at the wound site. Herein, the membranes capacity to adsorb fluids was characterized through the analysis of the swelling profile. For that purpose, the membranes were incubated in PBS at pH 5 (Figure 15C) and pH 8 (Figure 15D), to simulate the pH values of the native and injured skin, respectively [77, 107]. The obtained results show that the membranes have the maximum water uptake capacity after 24h of incubation, for both pHs. However, it is quite notorious that the swelling ratio for PVA_Lys, PVA_Lys_IBP, and PVA_Lys_LO membranes was higher at pH 5 (≈18.51, ≈17.10, ≈31.14) than at pH 8 (≈15.69, ≈10.51, ≈24.68), respectively. The membranes swelling behavior is related with the hydrophilicity of its raw materials (PVA and Lys), as well as the protonation/deprotonation of Lys functional groups associated with the pH variation. In fact, the Lys α-amino groups will be deprotonated at pH 8, yielding a neutral charge (≈ 0) to the Lys molecule [86, 151]. When the membrane is incubated at pH 5, the amino groups become protonated, leading to an increased electrostatic repulsion between them and, consequently, facilitating the establishment of stronger H-bonds with the water molecules (*i.e.* swelling occurs) [152].

Considering all the gathered data, the swelling capacity exhibited by the membranes highlights their potential to remove the excess of exudate from the wound, contributing for providing a suitable environment for the healing process to occur.

3.6. Determination of water vapor transmission rate of membranes

The wound dressings must also be permeable to moisture and gases in order to provide the optimal environment for the healing process [153]. In this way, the determination of the membranes' WVTR revealed that the PVA_Lys membranes present a WVTR of 1660.75 ± 171.58 mL/m^2/day, whereas the PVA_Lys_IBP and PVA_Lys_LO membranes display a WVTR of 1572.50 ± 151.74 mL/m^2/day and 1397.37 ± 220.44 mL/m^2/day, respectively. These data show that the incorporation of both biomolecules (IBP and LO) into the PVA_Lys membrane promote a decrease on its WVTR values. However, these values are still superior to those presented by the majority of the commercial available wound dressings (*e.g.* 285 ± 8 g/m^2/day for Comfeel (Coloplast A/S); 394 ± 12 g/m^2/day for Bioclusive (Johnson-Johnson); 792 ± 32 g/m^2/day for Op Site (Smith & Nephew) [154] and 120 ± 30 g/m^2/day for PVA-based asymmetric membranes [107])). Furthermore, these results are in agreement with other previously reported for electrospun membranes (*e.g.* 1713 ± 26 mL/m^2/day for CS_Arginine membranes [128],

1762.91 ± 187.50 mL/m^2/day for PCL_Hyaluronic acid/ CS_zein bilayer membrane [76], and 1353 g/m^2/day for CS electrospun membranes [155]).

3.7. Characterization of membranes' wettability through the measurement of water contact angles

The determination of the WCA at the surface of the electrospun membranes provide important insights about the host tissue interaction with the material surface. According to the literature, a hydrophilic surface displays a WCA < 90°, a moderate hydrophilic surface present a WCA higher than 40° and lower than 70°, a hydrophobic substrate possesses a WCA > 90°, while a super hydrophilic surface present a WCA < 10°[156, 157]. Herein, the PVA_Lys, PVA_Lys_IBP, and PVA_Lys_LO membranes exhibited a WCA of 32.38 ± 2.69°, 55.05 ± 2.55° and 63.83 ± 1.43°, respectively (as can be observed in Figure 16A). The PVA_Lys membrane presents the lower WCA, revealing a higher hydrophilic character. Such is justified by the presence of PVA and Lys in the composition of the membrane, which are both composed of highly hydrophilic groups [85]. On the other side, the IBP and LO incorporation promoted an increase on the WCA, resulting from the hydrophobic character of the incorporated molecules [126, 158]. However, the WCA values obtained for these two groups are comprehended between 40° and 70°, corresponding to a moderate hydrophilic character, which is considered to be suitable for encouraging the cell attachment and proliferation [69, 157].

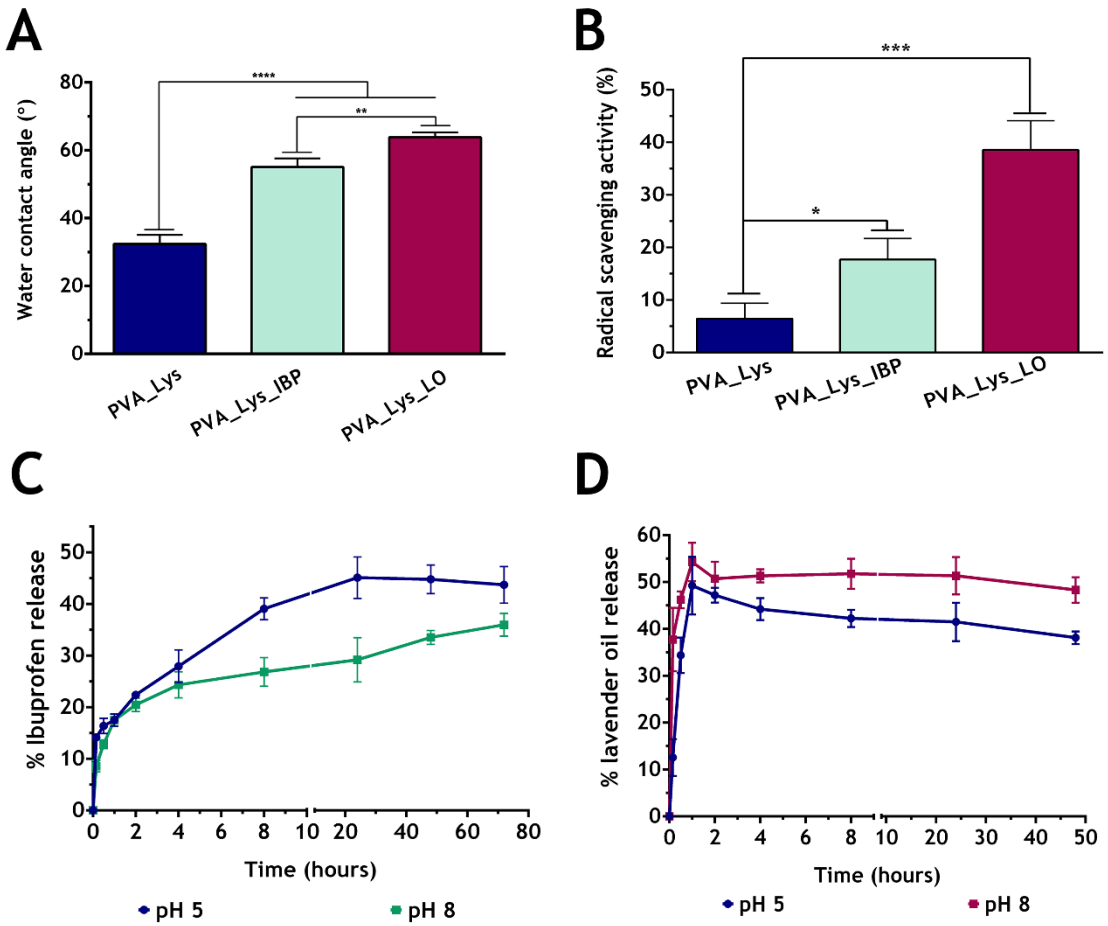

Figure 16. Characterization of physicochemical properties of the produced membranes. Determination of the electrospun membranes' water contact angles (A); Evaluation of the membranes' antioxidant activity (B); Characterization of the IBP (C) and LO (D) *in vitro* release profile at pH 5 and pH 8. (Data are presented as the mean ± standard deviation, n = 5, *p< 0.05, **p<0.001, ***p<0.0001 and ****p<0.00001).

3.8. Evaluation of the antioxidant activity of the membranes

There is a well-known relation between the inflammatory phase of the wound healing process and the exuberant production of reactive oxygen species (ROS). Imbalances on ROS production and their elimination may originate a condition of oxidative stress, which is commonly observed in chronic inflammatory diseases [159]. The ROS can trigger the pro-inflammatory cytokines secretion and the activity of matrix metalloproteases, which degrade the ECM, and consequently impairs the healing process.

In this work, the electrospun membranes were incubated with a solution containing DPPH radicals and their radical scavenging activity was evaluated (Figure 16B). The PVA_Lys exhibit a radical scavenging activity of 6.42 ± 2.94%, whereas the PVA_Lys_IBP and PVA_Lys_LO present higher radical scavenging values, 17.68 ± 3.99% and 38.54 ± 5.58%, respectively. The antioxidant activity of IBP is attributed to the presence of a phenyl group, which display scavenging activity for ROS [160]. Further, *in vivo* the IBP also decreases the ROS formation by inhibiting the COXs [161, 162]. In turn, the membranes containing the LO were the ones that showed the highest

antioxidant activity. The LO is an essential oil that has been widely applied in food processing due to its antioxidant activity, which is crucial for conferring protection to food products against oxidative rancidity [163, 164]. The LO' antioxidant activity arises from the presence of phenolic compounds in its composition, which act as free radical acceptors that delay/inhibit the autoxidation initiation step or prevents its propagation [165, 166].

3.9. Characterization of drug release profiles of IBP and LO from nanofibers

The intrinsic morphological properties of electrospun nanofibers combined with the versatility of the electrospinning technique constitute an attractive strategy to produce wound dressings able to provide protection to wound site and, simultaneously, deliver biomolecules that improve/accelerate the healing process [66, 93, 167]. Herein, IBP and LO were selected to be incorporated into PVA_Lys electrospun membranes, for providing anti-inflammatory, antibacterial or antioxidant properties. The EE and LE values obtained for IBP were 84.30 ± 5.81% and 71.77 ± 7.77%, whereas for LO were 83.42 ± 2.69% and 68.63 ± 9.77%, respectively. Such results revealed that both IBP and LO can be efficiently incorporated into PVA_Lys nanofibrous membrane through the electrospinning technique or surface physical adsorption methodologies, respectively.

Then, the IBP and LO release profiles from PVA_Lys nanofibrous membrane were characterized at pH 5 (found in native skin) and pH 8 (injured skin). The results obtained for IBP release from the nanofibers, at both pHs, show that the release occurred in a gradual manner reaching its maximum after 24 h of incubation, 45.09 ± 4.02% and 29.17 ± 4.29% of IBP were released at pH 5 and pH 8, respectively (Figure 16C). The impact of the pH on the IBP release profile is in accordance with the higher swelling exhibited by the membranes at pH 5, which facilitate, the drug diffusion from the nanofiber polymeric matrix to the external media.

On the other side, the LO release profile (Figure 16D) is characterized by an initial burst release that occurs in the first 4 h of immersion in PBS (34.21 ± 2.33% and 35.62 ± 6.13% at pH 5 and pH 8, respectively), followed by a stabilization of the drug release until 48 h. The LO burst release is justified by the method used to perform its incorporation into PVA_Lys membrane. In fact, the surface physical adsorption method used just promotes the LO immobilization on the surface of the polymeric matrix through electrostatic interactions (positively charged amine groups of Lys and negatively charged terpene groups available on LO structure) [126, 146-148]. Therefore, the LO will be immediately released from the nanofibers' surface, which is crucial to prevent the bacterial infections that usually occur within the first hours after the wound dressing application [168].

Further, the release data attained for the two biomolecules were also analysed by different mathematical kinetic models to confirm the type of interactions that are affecting its release (Table 4). In the case of IBP, the mathematical model that presents the best fitting for the data is the Korsmeyer-Peppas (R^2= 0.99 (n<0.5)). The fitting of the dot show that the IBP is released from the PVA_Lys membrane through a Fickian diffusion process, which occurs through the swelling of the polymeric matrix and the formation of heterogenous regions with a quicker drug dissolution in the composite nanofiber. Moreover, the IBP release also followed the first order kinetics (R^2= 0.99), corroborating the matrix dissolution-controlled release rate and further indicating that the drug release is dependent on the IBP concentration [107, 169]. On the other side, the Higuchi mathematical model provide the best fitting for the LO release profile. Such corroborates that the initial burst release occurs due to the diffusion of the LO molecules located at nanofibers' surface [169]. Therefore, it can be concluded that the incorporation method can be used to tailor the drug release profile in order to increase the biomolecule biological performance. For instance, the IBP controlled release profile is ideal to act during the inflammatory phase (1-3 days after injury), whereas the LO burst release is desirable for avoiding the initial bacterial contamination.

Table 4. Regression coefficients obtained by applying the mathematical models to fit the release of IBP and LO from the PVA_Lys nanofibrous membrane at pH 5 and pH 8.

		First order	Higuchi	Korsmeyer-Peppas	
		R^2	R^2	R^2	n
pH 5	**IBP**	0.98		0.99	0.11
pH 8		0.99		0.99	0.37
pH 5	**LO**		0.99	0.95	0.20
pH 8			0.99	0.96	0.27

3.10. Characterization of biological properties of the electrospun membranes

The biological properties of the electrospun membranes were evaluated using the NHDF as model cells. These cells were selected due to their pivotal role in wound healing process [170]. They are responsible for the production of collagen, growth factors, adhesive molecules, and cytokines that regulate the reestablishment of the injured skin [170]. The optical microscopic images of NHDF cells seeded in contact with electrospun membranes were acquired after 1, 3 and 7 days of incubation (Figure 17). The images show that the cell morphology was not affected by the presence of PVA_Lys membranes, since they exhibit an elongated morphology quite similar to those cells found in the negative control (*i.e.* cells incubated just with culture medium).

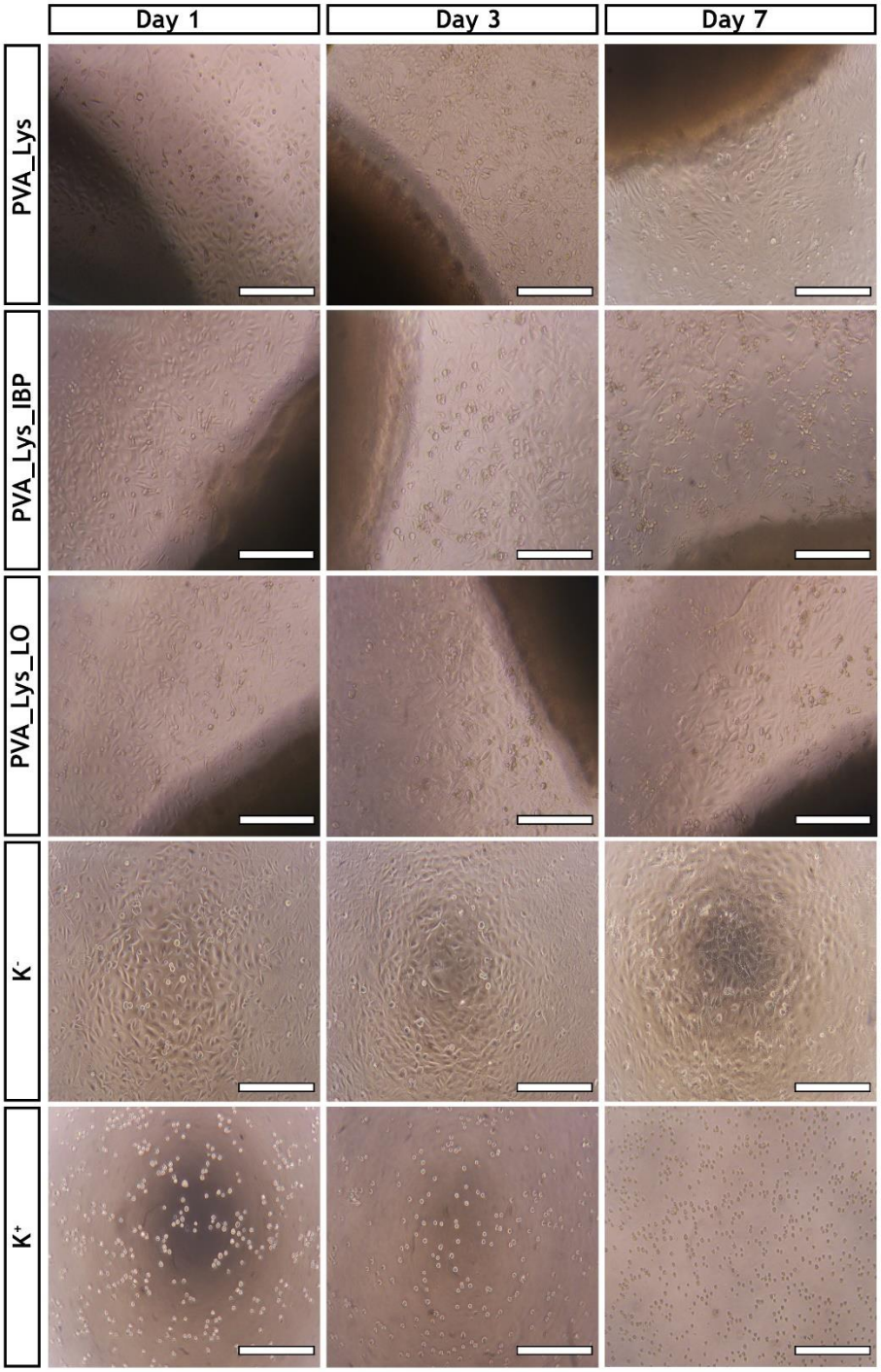

Figure 17. Optical microscopic images of NHDF cells cultured in the presence of the produced membranes (PVA_Lys, PVA_Lys_IBP and PVA_Lys_LO) after 1, 3, and 7 days of incubation; K^- (negative control); K^+ (positive control). Scale bar represents 200 µm.

Additionally, the membranes' cytotoxic profile was analysed through an MTS assay over 1, 3, and 7 days (Figure 18A). The obtained data indicate that all the produced membranes did not induce any cytotoxic effect on NHDFs, over the 7 days. Further the concentration of IBP (1mg/mL) and LO (1.3 mg/mL) incorporated into the nanofibers did not compromise fibroblasts' viability. Likewise, membranes' biocompatibility was also further evaluated through a dsDNA

assay, where the results show that no significant differences were noticed in dsDNA content of cells in contact with membranes or just in the presence of culture medium over a period of 7 days (Figure 18B).

Moreover, the SEM images (Figure 18C) evidenced the bioadhesive properties of the electrospun membranes, showing that the cells adhered and spread at the surface of the membranes, along 7 days of incubation. Such occur essentially due to the presence of positively charged amine groups on Lys backbone (in membranes composition), which interact with negatively charged glycosaminoglycans found in cell membrane [171]. In fact, the Lys and their derivatives have been commonly used to perform the coating of the cell culture dishes' surface due to their biocompatibility, cell adhesion capacity, and relatively good solubility in water [87].

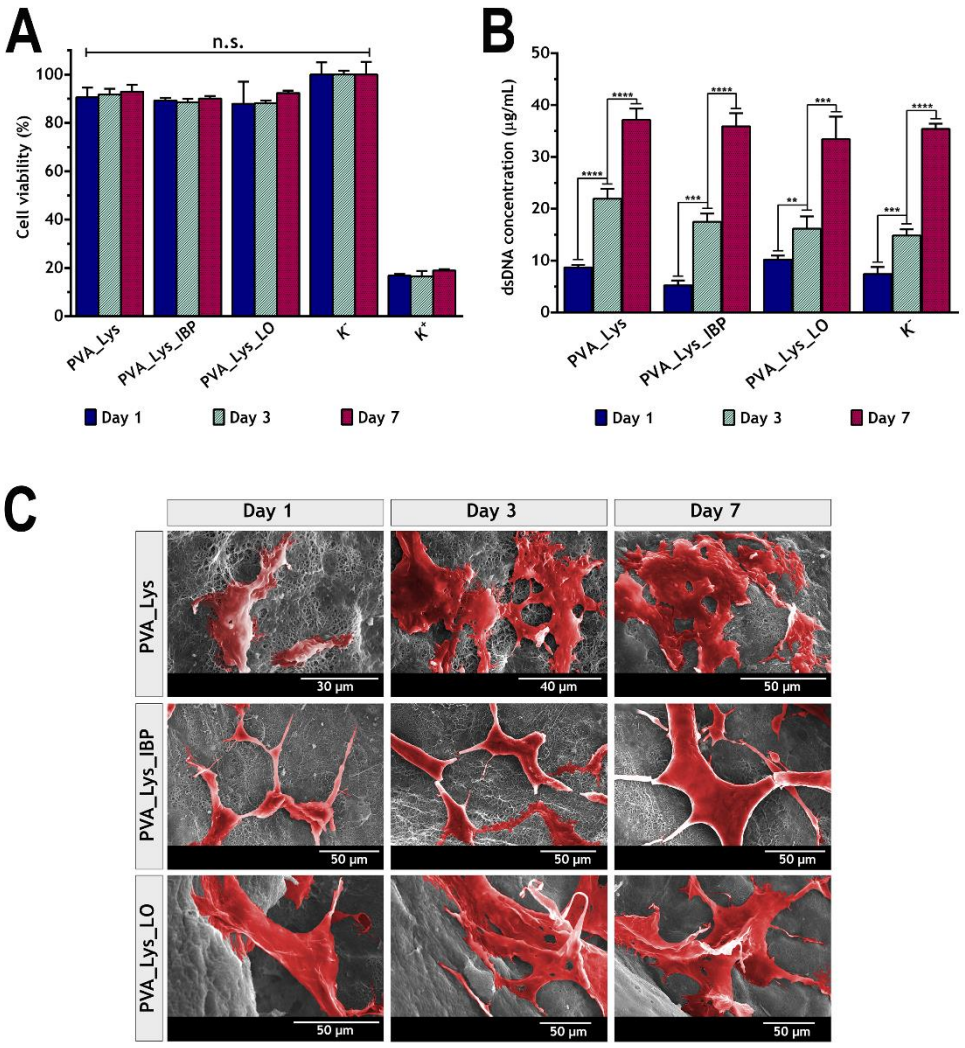

Figure 18. Characterization of the electrospun membranes' biocompatibility. Analysis of the NHDF cell viability using an MTS assay (A) and by determining dsDNA content (B) after 1, 3, and 7 days of incubation with the membranes. Data are presented as the mean ± standard deviation, n = 5, **p< 0.01, ***p< 0.001, and ****p< 0.0001. SEM images of NHDF cells seeded at the surface of the electrospun membranes after 1, 3, and 7 days (C).

Furthermore, the Live/Dead assays allow to characterize the cell survival at the membranes' surface, by simultaneously staining both live (green labelled) and dead (red labelled) cells with Calcein and Propidium iodide, respectively. The confocal microscopy images (Figure 19) demonstrated that the fibroblasts remain viable and their number increase along time, corroborating the results obtained in the MTS and dsDNA assays.

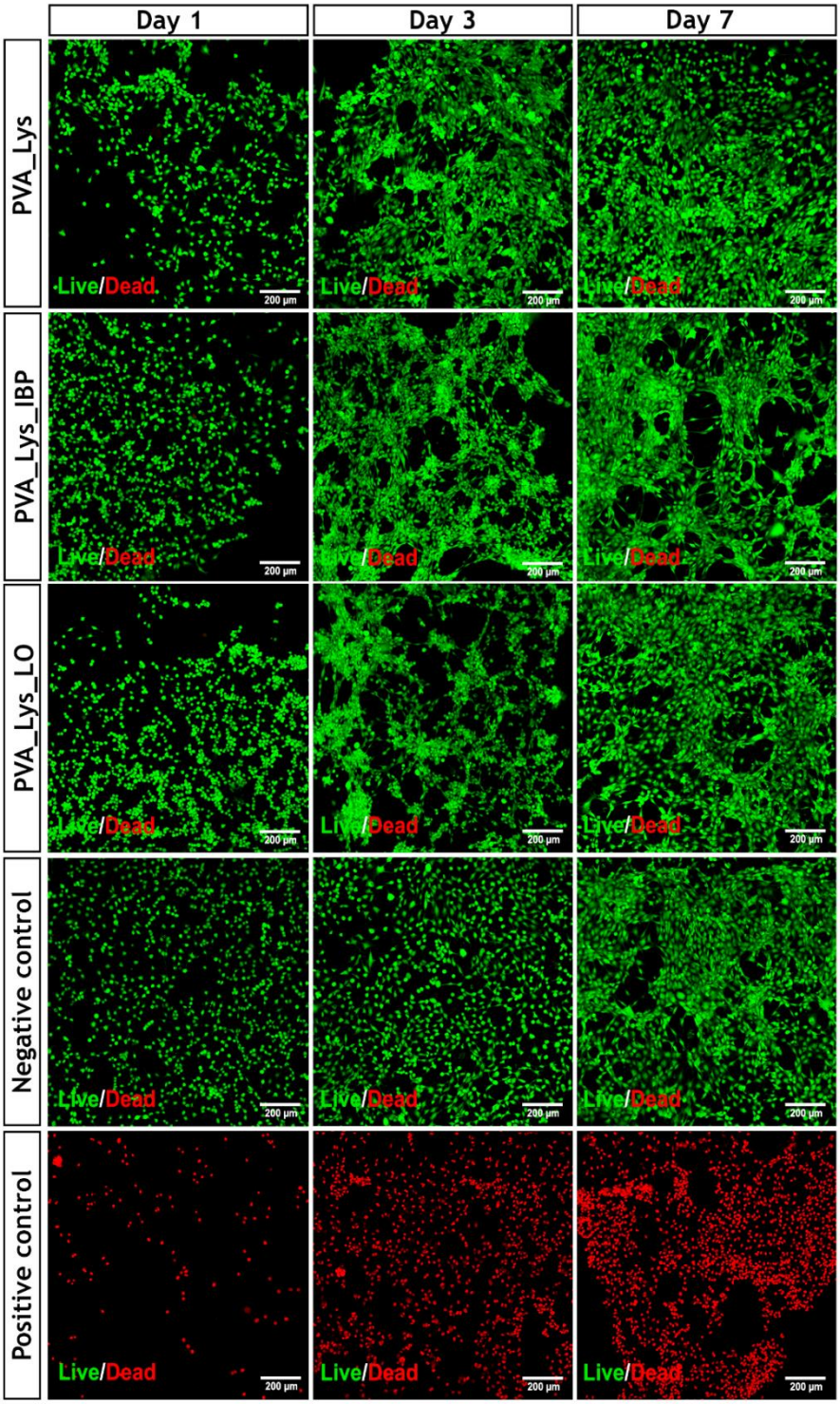

Figure 19. Fluorescence microscopic images of Live/Dead assay: NHDFs cultured on electrospun membranes' surface after, 1, 3 and 7 days. Green channel: viable cells labelled with Calcein; red channel: dead cells stained with Propidium iodide.

In addition, the cell proliferation, attachment and migration into the membranes were also characterized through CLSM analysis (Figure 20). The results revealed that the fibroblast cells maintained a normal phenotype and remained biologically active at the surface of electrospun membranes during 3 days, corroborating the data obtained through SEM analysis. Further, the

color coded depth analysis of the membranes indicated that fibroblasts migrated within the electrospun membranes, with cells localized between 30-60 µm of depth within the membranes' polymeric matrix. Overall, the obtained data clearly demonstrate the excellent biocompatibility of the PVA_Lys electrospun membranes based-drug delivery systems, encouraging their application as wound dressings.

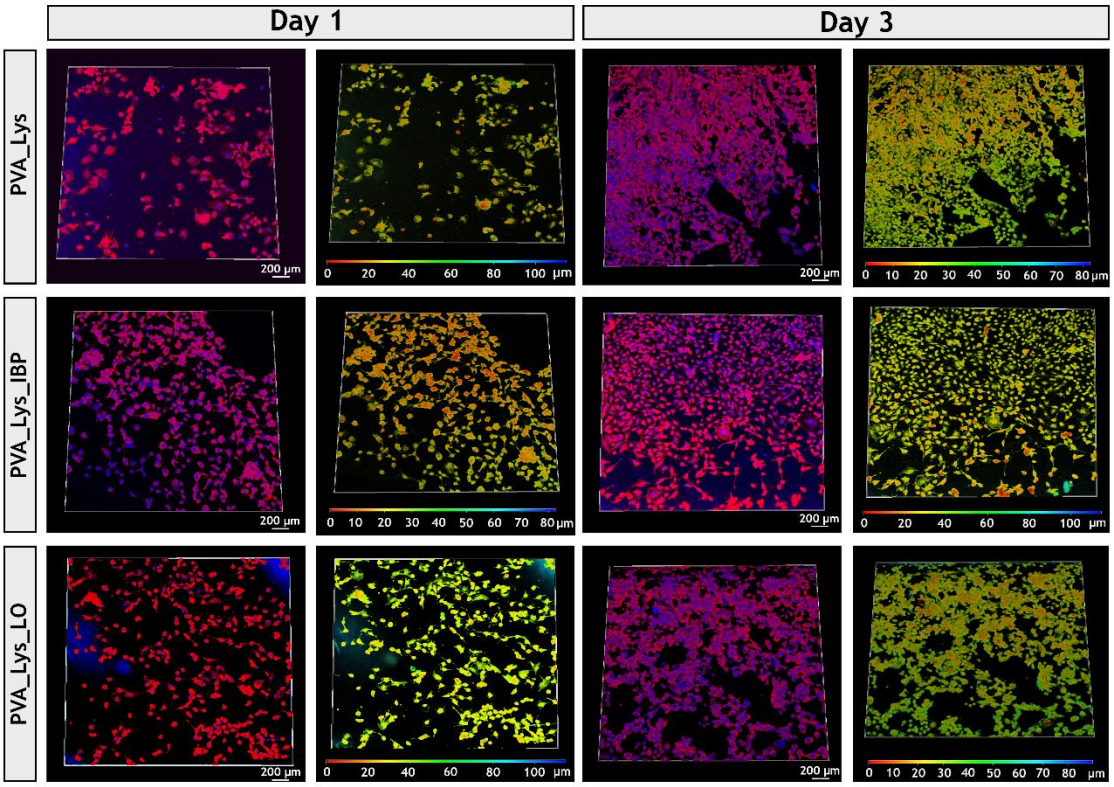

Figure 20. CLSM images of NHDF cultured on the electrospun membranes' surface (PVA_Lys, PVA_Lys_IBP and PVA_Lys_LO). Color coded depth analysis of NHDF penetration on the membrane (red 0 µm, blue 80–100 µm) after 1 and 3 days. Blue channel: cell nuclei labelled Hoechst 33342®; red channel: cytoplasm stained with WGA-Alexa 594®.

3.11. Evaluation of antimicrobial properties of the electrospun membranes

An open wound provides a favourable niche for microbial colonization, which will impair the healing process. Additionally, the microbial infections are one of the main causes of a high rates of morbidity and mortality associated with the wound management. So, the development of wound dressings displaying antimicrobial activity is crucial to avoid bacterial penetration and infections. Herein, the membranes' antimicrobial properties were evaluated against *S.aureus* (Gram-positive bacteria) and *P.aeruginosa* (Gram-negative bacteria). These strains were chosen since they are the most common microorganisms found in skin infections [172].

The obtained results showed that the different PVA_Lys membranes can impair or even inhibit bacteria growth. The PVA_Lys, PVA_Lys_IBP, and PVA_Lys_LO induced bacteria growth inhibition of 34.55 ± 7.87%, 34.85 ± 4.48%, and 96.96 ± 1.84% for *S.aureus*, and 25.00 ± 2.90%, 21.00 ± 8.23%, and 91.18 ± 7.88% for *P.aeruginosa*, respectively (as can be observed in Figures 21A and 21B). Similar results were observed in the agar diffusion assay, with the PVA_Lys, PVA_Lys_IBP and PVA_Lys_LO membranes (Figure 21C) presenting an inhibitory area of 20.43± 5.78%, 20.49 ± 3.42% and 61.76 ± 11.75% against *S.aureus* and 0.51 ± 0.01%, 0.45 ±0.02% and 32.77 ± 1.36% for *P.aeruginosa*, respectively. Additionally, SEM images (Figure 22) also showed that no biofilm formation occurred at PVA_Lys, PVA_Lys_IBP and PVA_Lys_LO membranes' surface when samples were incubated with *S.aureus*. On the other hand, when membranes were incubated with *P.aeruginosa*, biofilm formation was only inhibited at the surface of PVA_Lys_LO membrane.

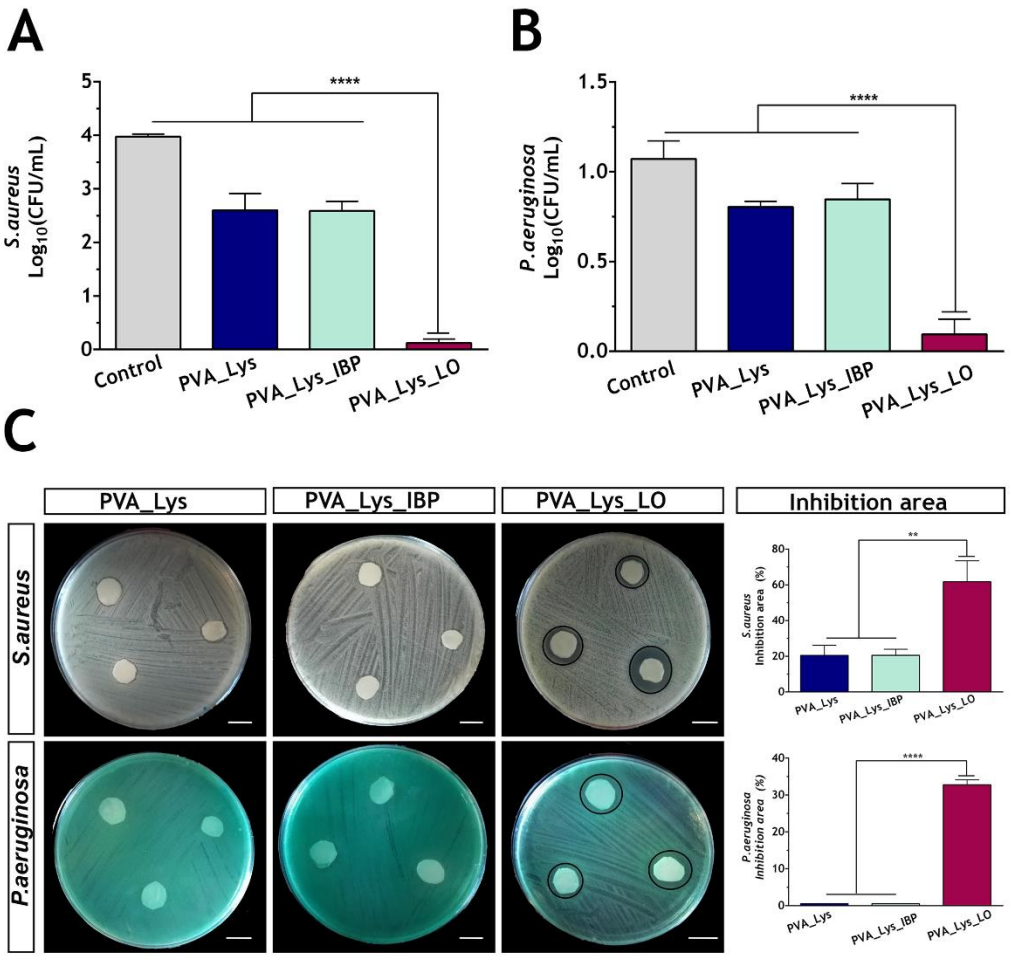

Figure 21. Evaluation of the produced membranes antibacterial activity. Determination of the CFU/mL of *S.aureus* (A) and *P.aeruginosa* (B), when membranes were added to the cultures. Macroscopic images and analysis of the inhibitory halos against *S.aureus* and *P.aeruginosa* formed by the produced membranes (C). Data are presented as the mean ± standard deviation, n = 5, **p<0.001, ****p< 0.0001.

These results are in agreement with the antibacterial properties already reported in the literature for LO [173, 174]. The antibacterial activity presented by LO is justified by the phenolic compounds (*e.g.* linalool, linalyl acetate, 1,8-cineole, ß-ocimene, terpinen-4-ol) found in their composition. Furthermore, the electronegative compounds present on LO' composition will also interfere on the bacteria biological processes (*e.g.* electron transfer, protein translocation, phosphorylation steps) and therefore inhibit the growth of bacteria [126, 146]. On the other hand, the essential oils can also disrupt the bacterial cell wall and cytoplasmic membrane leading to the cell lysis and subsequent leakage of intracellular compounds [175, 176]. However, in this work, the antibacterial activity of LO was influenced by the microorganisms' structure, *i.e.* the PVA_Lys_LO presented an enhanced antibacterial effect against *S.aureus*. This result may be explained by the presence of a more complex and rigid cell wall on gram-negative bacteria, which is mainly composed of lipopolysaccharides that decrease the diffusion of hydrophobic compounds, such as the essential oils [77, 118]. On the other side, the antibacterial activity obtained for PVA_Lys and PVA_Lys_IBP membranes against *S.aureus* can be attributed to the interaction of the positively charged amine groups of Lys with the negatively charged groups available on bacteria' surface, which will lead to an increased cell wall permeability and, consequently, to the leakage of intracellular compounds [177].

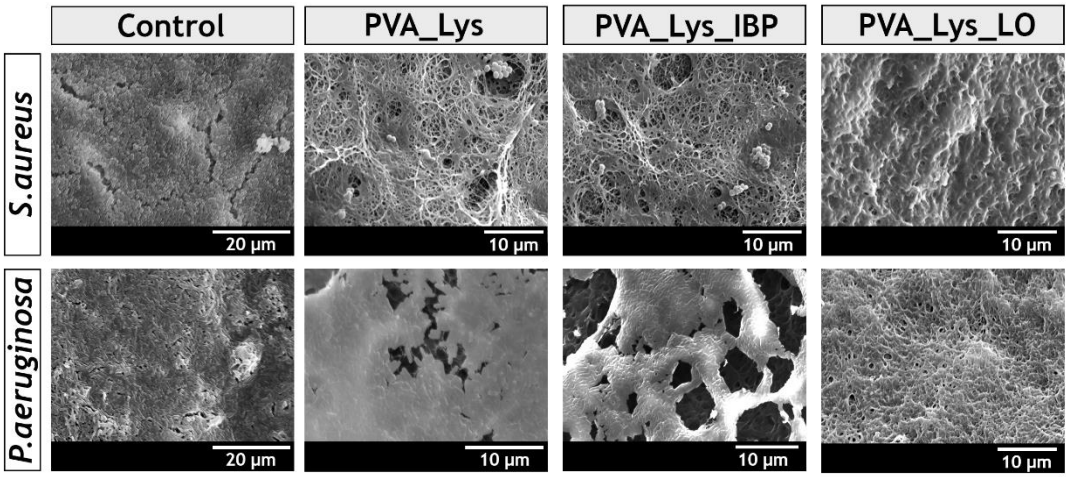

Figure 22. SEM images of control, PVA_Lys, PVA_Lys_IBP and PVA_Lys_LO membranes incubated with *S.aureus* and *P.aeruginosa*.

Chapter IV - Conclusion and Future Perspectives

4. Conclusions and Future Perspectives

Nowadays, skin lesions continue to represent a huge health problem for the worldwide population. Further, the actual therapeutic strategies are unable to reproduce all structural and functional features of native skin. Among the different therapies under development, the electrospun membranes have gained a special attention in the skin regeneration area, since they possess similar morphology and structure to that of skin ECM. Furthermore, the incorporation of biomolecules into nanofibrous structures can be performed through different techniques that allow the tailoring of the release profile of a bioactive molecule, to answer to specific demands of the healing process.

Herein, a new nanofibrous membrane was produced with PVA and Lys using the electrospinning technique. In addition, IBP and LO were incorporated within the nanofibers to confer them anti-inflammatory and antibacterial/antioxidant properties, respectively. The biomolecules incorporation was achieved by using different methodologies in order to obtain distinct release profiles, *i.e.*, IBP was incorporated through blend electrospinning to obtain a controlled and sustained drug release profile, whereas the LO was adsorbed at membrane' surface using a physical adsorption method. This method was used to achieve a burst initial release of LO.

In this way, a controlled and sustained release of IBP will allow to control the inflammatory phase, while the initial burst release of LO will provide an initial asseptic environment at wound site, in order to avoid the bacterial colonization.

The gathered data showed that all the electrospun membranes presented suitable morphological, mechanical, physicochemical and biological properties to be used as wound dressing. Moreover, the LO incorporation granted antimicrobial properties to the PVA_Lys membrane, since the membranes were able to inhibit the growth of *S.aureus* and *P.aeruginosa*, without compromising fibroblasts viability.

In the near future, the anti-inflammatory activity of IBP will be evaluated *in vitro* (*i.e.* through the quantification of IL-6 and IL-1ß and TNF-α cytokines) as well as through *in vivo* assays to validate the potential of this wound dressing in the control of the inflammatory phase during the healing process. Moreover, the synergic effect of the IBP and LO incorporation into the same electrospun membrane will be further characterized to support the application of this multifunctional wound dressing.

Chapter V - References

5. References

1. Vig, K., et al., *Advances in skin regeneration using tissue engineering*. International journal of molecular sciences, 2017. **18**(4): p. 789.
2. Aljghami, M.E., S. Saboor, and S. Amini-Nik, *Emerging Innovative Wound Dressings*. Annals of Biomedical Engineering, 2019. **47**(3): p. 659-675.
3. Guerra, A., J. Belinha, and R.N. Jorge, *Modelling skin wound healing angiogenesis: A review*. Journal of theoretical biology, 2018. **459**: p. 1-17.
4. Khavkin, J. and D.A. Ellis, *Aging skin: histology, physiology, and pathology*. Facial Plastic Surgery Clinics, 2011. **19**(2): p. 229-234.
5. Tobin, D.J., *Introduction to skin aging*. Journal of tissue viability, 2017. **26**(1): p. 37-46.
6. https://commons.wikimedia.org/wiki/File:Burns.png. (Acessed in 03/06/2019)
7. Wikramanayake, T.C., O. Stojadinovic, and M. Tomic-Canic, *Epidermal differentiation in barrier maintenance and wound healing*. Advances in wound care, 2014. **3**(3): p. 272-280.
8. Yannas, I.V., *Tissue and organ regeneration in adults*. Vol. 10. 2001: Springer.
9. Kolarsick, P.A., M.A. Kolarsick, and C. Goodwin, *Anatomy and physiology of the skin*. Journal of the Dermatology Nurses' Association, 2011. **3**(4): p. 203-213.
10. Zhang, Z. and B.B. Michniak-Kohn, *Tissue engineered human skin equivalents*. Pharmaceutics, 2012. **4**(1): p. 26-41.
11. https://smart.servier.com. (Acessed in 03/06/2019)
12. Losquadro, W.D., *Anatomy of the Skin and the Pathogenesis of Nonmelanoma Skin Cancer*. Facial Plastic Surgery Clinics, 2017. **25**(3): p. 283-289.
13. Lai-Cheong, J.E. and J.A. McGrath, *Structure and function of skin, hair and nails*. Medicine, 2009. **37**(5): p. 223-226.
14. Venus, M., J. Waterman, and I. McNab, *Basic physiology of the skin*. Surgery (Oxford), 2010. **28**(10): p. 469-472.
15. Boateng, J. and O. Catanzano, *Advanced therapeutic dressings for effective wound healing—a review*. Journal of pharmaceutical sciences, 2015. **104**(11): p. 3653-3680.
16. Zahedi, P., et al., *A review on wound dressings with an emphasis on electrospun nanofibrous polymeric bandages*. Polymers for Advanced Technologies, 2010. **21**(2): p. 77-95.
17. Ho, J., et al., *Current advancements and strategies in tissue engineering for wound healing: a comprehensive review*. Advances in wound care, 2017. **6**(6): p. 191-209.
18. Sen, C.K., et al., *Human skin wounds: a major and snowballing threat to public health and the economy*. Wound repair and regeneration, 2009. **17**(6): p. 763-771.
19. Zhao, R., et al., *Inflammation in chronic wounds*. International journal of molecular sciences, 2016. **17**(12): p. 2085.

20. Rittié, L., *Cellular mechanisms of skin repair in humans and other mammals.* Journal of cell communication and signaling, 2016. **10**(2): p. 103-120.
21. Shevchenko, R.V., S.L. James, and S.E. James, *A review of tissue-engineered skin bioconstructs available for skin reconstruction.* Journal of the royal Society Interface, 2009. **7**(43): p. 229-258.
22. Eming, S.A., P. Martin, and M. Tomic-Canic, *Wound repair and regeneration: mechanisms, signaling, and translation.* Science translational medicine, 2014. **6**(265): p. 265sr6-265sr6.
23. Reinke, J. and H. Sorg, *Wound repair and regeneration.* European surgical research, 2012. **49**(1): p. 35-43.
24. Gurtner, G.C., et al., *Wound repair and regeneration.* Nature, 2008. **453**(7193): p. 314-321.
25. Miguel, S.P., et al., *Electrospun polymeric nanofibres as wound dressings: a review.* Colloids and surfaces B: Biointerfaces, 2018. **169**: p. 60-71.
26. Rodrigues, M., et al., *Wound healing: a cellular perspective.* Physiological reviews, 2018. **99**(1): p. 665-706.
27. Rieger, K.A., N.P. Birch, and J.D. Schiffman, *Designing electrospun nanofiber mats to promote wound healing–a review.* Journal of Materials Chemistry B, 2013. **1**(36): p. 4531-4541.
28. Bielefeld, K.A., S. Amini-Nik, and B.A. Alman, *Cutaneous wound healing: recruiting developmental pathways for regeneration.* Cellular and Molecular Life Sciences, 2013. **70**(12): p. 2059-2081.
29. https://www.biodermis.com/what-are-the-stages-of-wound-healing-s/221.htm. (Acessed in 03/06/2019)
30. https://www.who.int/news-room/fact-sheets/detail/burns. ((Acessed in 03/06/2019)
31. Boyce, S.T. and G.D. Warden, *Principles and practices for treatment of cutaneous wounds with cultured skin substitutes.* The American journal of surgery, 2002. **183**(4): p. 445-456.
32. Phillips, T.J., *Current approaches to venous ulcers and compression.* Dermatologic surgery, 2001. **27**(7): p. 611-621.
33. Rakhshaei, R. and H. Namazi, *A potential bioactive wound dressing based on carboxymethyl cellulose/ZnO impregnated MCM-41 nanocomposite hydrogel.* Materials Science and Engineering: C, 2017. **73**: p. 456-464.
34. Catalano, E., et al., *Tissue-engineered skin substitutes: an overview.* Journal of Artificial Organs, 2013. **16**(4): p. 397-403.
35. Rowan, M.P., et al., *Burn wound healing and treatment: review and advancements.* Critical care, 2015. **19**(1): p. 243.
36. Atiyeh, B.S., S.N. Hayek, and S.W. Gunn, *New technologies for burn wound closure and healing—review of the literature.* Burns, 2005. **31**(8): p. 944-956.

37. Dvir, T., et al., *Nanotechnological strategies for engineering complex tissues.* Nature nanotechnology, 2011. **6**(1): p. 13-22.
38. Savoji, H., et al., *Skin tissue substitutes and biomaterial risk assessment and testing.* Frontiers in bioengineering and biotechnology, 2018. **6**(86).
39. Moustafa, M., et al., *Randomized, controlled, single-blind study on use of autologous keratinocytes on a transfer dressing to treat nonhealing diabetic ulcers.* Regenerative Medicine, 2007. **2**(6): p. 887-902.
40. Rahmanian-Schwarz, A., et al., *A clinical evaluation of Biobrane® and Suprathel® in acute burns and reconstructive surgery.* Burns, 2011. **37**(8): p. 1343-1348.
41. Park, S., Y. Kim, and S. Jang, *The application of an acellular dermal allograft (AlloDerm) for patients with insufficient conjunctiva during evisceration and implantation surgery.* Eye, 2018. **32**(1): p. 136-141.
42. Kamel, S., *One-stage vs two-stage implant placement: A systematic review and meta-analysis.* British Journal of Oral and Maxillofacial Surgery, 2018. **56**(10): p. e25.
43. delli Santi, G., et al., *The use of dermal regeneration template (Matriderm® 1 mm) for reconstruction of a large full-thickness scalp and calvaria exposure.* Journal of Burn Care & Research, 2016. **37**(5): p. e497-e498.
44. Romanelli, M., V. Dini, and M.S. Bertone, *Randomized comparison of OASIS wound matrix versus moist wound dressing in the treatment of difficult-to-heal wounds of mixed arterial/venous etiology.* Advances in skin & wound care, 2010. **23**(1): p. 34-38.
45. Hart, C.E., A. Loewen-Rodriguez, and J. Lessem, *Dermagraft: use in the treatment of chronic wounds.* Advances in wound care, 2012. **1**(3): p. 138-141.
46. Kumar, R.J., et al., *Treatment of partial-thickness burns: a prospective, randomized trial using TranscyteTM.* ANZ journal of surgery, 2004. **74**(8): p. 622-626.
47. Myers, S.R., et al., *Hyalomatrix: a temporary epidermal barrier, hyaluronan delivery, and neodermis induction system for keratinocyte stem cell therapy.* Tissue Engineering 2007. **13**(11): p. 2733-2741.
48. Edmonds, M. and E.a.A.A.D.F.U.S. Group., *Apligraf in the treatment of neuropathic diabetic foot ulcers.* The International Journal of Lower Extremity Wounds, 2009. **8**(1): p. 11-18.
49. Still, J., et al., *The use of a collagen sponge/living cell composite material to treat donor sites in burn patients.* Burns, 2003. **29**(8): p. 837-841.
50. MacNeil, S., *Progress and opportunities for tissue-engineered skin.* Nature, 2007. **445**(7130): p. 874-880.
51. Varkey, M., J. Ding, and E.E. Tredget, *Advances in Skin Substitutes-Potential of Tissue Engineered Skin for Facilitating Anti-Fibrotic Healing.* Journal of functional biomaterials, 2015. **6**(3): p. 547-563.
52. Boateng, J.S., et al., *Wound healing dressings and drug delivery systems: a review.* Journal of pharmaceutical sciences, 2008. **97**(8): p. 2892-2923.

53. Ramos-e-Silva, M. and d.C.M. Ribeiro, *New dressings, including tissue-engineered living skin.* Clinics in dermatology, 2002. **20**(6): p. 715-723.
54. Caló, E. and V.V. Khutoryanskiy, *Biomedical applications of hydrogels: A review of patents and commercial products.* European Polymer Journal, 2015. **65**: p. 252-267.
55. Ahmed, E.M., *Hydrogel: Preparation, characterization, and applications: A review.* Journal of advanced research, 2015. **6**(2): p. 105-121.
56. Kamoun, E.A., E.S. Kenawy, and X. Chen, *A review on polymeric hydrogel membranes for wound dressing applications: PVA-based hydrogel dressings.* Journal of advanced research, 2017. **8**(3): p. 217-233.
57. Pott, F.S., et al., *The effectiveness of hydrocolloid dressings versus other dressings in the healing of pressure ulcers in adults and older adults: a systematic review and meta-analysis.* Revista latino-americana de enfermagem, 2014. **22**(3): p. 511-520.
58. Bhattarai, S.R., et al., *Novel biodegradable electrospun membrane: scaffold for tissue engineering.* Biomaterials, 2004. **25**(13): p. 2595-2602.
59. Liu, M., et al., *Electrospun nanofibers for wound healing.* Materials Science & Engineering C, 2017. **76**: p. 1413-1423.
60. Pilehvar-Soltanahmadi, Y., et al., *An update on clinical applications of electrospun nanofibers for skin bioengineering.* Artificial Cells, Nanomedicine, and Biotechnology, 2016. **44**(6): p. 1350-1364.
61. Augustine, R., N. Kalarikkal, and S. Thomas, *Advancement of wound care from grafts to bioengineered smart skin substitutes.* Progress in Biomaterials, 2014. **3**(2-4): p. 103-113.
62. Abrigo, M., S.L. McArthur, and P. Kingshott, *Electrospun nanofibers as dressings for chronic wound care: advances, challenges, and future prospects.* Macromolecular bioscience, 2014. **14**(6): p. 772-792.
63. Xue, J., et al., *Electrospun Nanofibers: New Concepts, Materials, and Applications.* Accounts of Chemical Research, 2017. **50**(8): p. 1976-1987.
64. Pereira, R.F., et al., *Advanced biofabrication strategies for skin regeneration and repair.* Nanomedicine, 2013. **8**(4): p. 603-621.
65. Bhattarai, R.S., et al., *Biomedical Applications of Electrospun Nanofibers: Drug and Nanoparticle Delivery.* Pharmaceutics, 2018. **11**(1).
66. Braghirolli, D.I., D. Steffens, and P. Pranke, *Electrospinning for regenerative medicine: a review of the main topics.* Drug discovery today, 2014. **19**(6): p. 743-753.
67. Khil, M.S., et al., *Electrospun nanofibrous polyurethane membrane as wound dressing.* Journal of Biomedical Materials Research, 2003. **67**(2): p. 675-679.
68. Soares, R.M.D., et al., *Electrospinning and electrospray of bio-based and natural polymers for biomaterials development.* Materials Science & Engineering C, 2018. **92**: p. 969-982.

69. Miguel, S., et al., *Electrospun Polycaprolactone/aloe Vera_Chitosan Nanofibrous asymmetric membranes aimed for wound healing applications.* Polymers, 2017. **9**(5): p. 183.
70. Liu, B., et al., *Antibacterial PCL electrospun membranes containing synthetic polypeptides for biomedical purposes.* Colloids and Surfaces B: Biointerfaces, 2018. **172**: p. 330-337.
71. Perumal, G., et al., *Synthesis and characterization of curcumin loaded PLA-Hyperbranched polyglycerol electrospun blend for wound dressing applications.* Materials Science & Engineering C, 2017. **76**: p. 1196-1204.
72. Garcia-Orue, I., et al., *Composite nanofibrous membranes of PLGA/Aloe vera containing lipid nanoparticles for wound dressing applications.* International Journal of Pharmaceutics, 2019. **556**: p. 320-329.
73. Santos, C., et al., *Preparation and characterization of polysaccharides/PVA blend nanofibrous membranes by electrospinning method.* Carbohydrate polymers, 2014. **99**: p. 584-592.
74. Sell, S.A., et al., *Electrospinning of collagen/biopolymers for regenerative medicine and cardiovascular tissue engineering.* Advanced Drug Delivery Reviews, 2009. **61**(12): p. 1007-1019.
75. Jalaja, K., et al., *Potential of electrospun core-shell structured gelatin-chitosan nanofibers for biomedical applications.* Carbohydrate Polymers, 2016. **136**: p. 1098-1107.
76. Figueira, D.R., et al., *Production and characterization of polycaprolactone-hyaluronic acid/chitosan-zein electrospun bilayer nanofibrous membrane for tissue regeneration.* International journal of biological macromolecules, 2016. **93**: p. 1100-1110.
77. Miguel, S.P., et al., *Production and characterization of electrospun silk fibroin based asymmetric membranes for wound dressing applications.* International journal of biological macromolecules, 2019. **121**: p. 524-535.
78. Yuan, T.T., et al., *Development of Electrospun Chitosan-Polyethylene Oxide/Fibrinogen Biocomposite for Potential Wound Healing Applications.* Nanoscale Research Letters, 2018. **13**(1): p. 88.
79. Chen, K.Y., et al., *Synthesis and characterization of poly(vinyl alcohol) membranes with quaternary ammonium groups for wound dressing.* Journal of Biomaterials Science, Polymer Edition, 2010. **21**(4): p. 429-443.
80. Zhao, L., et al., *Synthesis of antibacterial PVA/CM-chitosan blend hydrogels with electron beam irradiation.* Carbohydrate Polymers, 2003. **53**(4): p. 439-446.
81. Yan, E., et al., *Electrospun polyvinyl alcohol/chitosan composite nanofibers involving Au nanoparticles and their in vitro release properties.* Materials Science and Engineering C, 2013. **33**(1): p. 461-465.

82. Kheradvar, S.A., et al., *Starch nanoparticle as a vitamin E-TPGS carrier loaded in silk fibroin-poly(vinyl alcohol)-Aloe vera nanofibrous dressing.* Colloids and Surfaces B: Biointerfaces, 2018. **166**: p. 9-16.
83. Mohseni, M., et al., *Antimicrobial Wound Dressing Containing Silver Sulfadiazine With High Biocompatibility: In Vitro Study.* Artificial Organs, 2016. **40**(8): p. 765-773.
84. Augustine, R., et al., *Electrospun polyvinyl alcohol membranes incorporated with green synthesized silver nanoparticles for wound dressing applications.* Journal of Materials Science: Materials in Medicine, 2018. **29**(11): p. 163.
85. Miao, Y., et al., *Poly (L-lysine) modified zein nanofibrous membranes as efficient scaffold for adhesion, proliferation, and differentiation of neural stem cells.* Royal Society of Chemistry Advances, 2017. **7**(29): p. 17711-17719.
86. Nolting, D., et al., *pH-induced protonation of lysine in aqueous solution causes chemical shifts in X-ray photoelectron spectroscopy.* Journal of the American Chemical Society, 2007. **129**(45): p. 14068-14073.
87. Wang, X., et al., *Highly efficient labeling of human lung cancer cells using cationic poly-l-lysine-assisted magnetic iron oxide nanoparticles.* Nano-micro letters, 2015. **7**(4): p. 374-384.
88. Heo, J.S., et al., *Poly-L-lysine Prevents Senescence and Augments Growth in Culturing Mesenchymal Stem Cells Ex Vivo.* BioMed Research International, 2016. **2016**: p. 1-13.
89. Lai, J.Y., et al., *Stabilization of collagen nanofibers with L-lysine improves the ability of carbodiimide cross-linked amniotic membranes to preserve limbal epithelial progenitor cells.* International journal of nanomedicine, 2014. **9**: p. 5117-5130.
90. Ding, Y., et al., *Electrospun Fibrous Architectures for Drug Delivery, Tissue Engineering and Cancer Therapy.* Advanced functional materials, 2018. **29**(2).
91. Leung, V. and F. Ko, *Biomedical applications of nanofibers.* Polymers for advanced technologies, 2011. **22**(3): p. 350-365.
92. Hu, X., et al., *Electrospinning of polymeric nanofibers for drug delivery applications.* Journal of controlled release, 2014. **185**: p. 12-21.
93. Miguel, S.P., et al., *An overview of electrospun membranes loaded with bioactive molecules for improving the wound healing process.* European Journal of Pharmaceutics and Biopharmaceutics, 2019. **139**: p. 1-22.
94. Im, J.S., et al., *Fluorination of electrospun hydrogel fibers for a controlled release drug delivery system.* Acta biomaterialia, 2010. **6**(1): p. 102-109.
95. Saraf, A., et al., *Regulated non-viral gene delivery from coaxial electrospun fiber mesh scaffolds.* Journal of Controlled Release, 2010. **143**(1): p. 95-103.
96. Zamani, M., M.P. Prabhakaran, and S. Ramakrishna, *Advances in drug delivery via electrospun and electrosprayed nanomaterials.* International journal of nanomedicine, 2013. **8**: p. 2997-3017.

97. Chou, S.-F., D. Carson, and K.A. Woodrow, *Current strategies for sustaining drug release from electrospun nanofibers.* Journal of Controlled Release, 2015. **220**: p. 584-591.
98. Grassi, M. and G. Grassi, *Mathematical modelling and controlled drug delivery: matrix systems.* Current drug delivery, 2005. **2**(1): p. 97-116.
99. Ji, W., et al., *Bioactive electrospun scaffolds delivering growth factors and genes for tissue engineering applications.* Pharmaceutical research, 2011. **28**(6): p. 1259-1272.
100. Preem, L. and K. Kogermann, *Electrospun Antimicrobial Wound Dressings: Novel Strategies to Fight Against Wound Infections*, in *Recent Clinical Techniques, Results, and Research in Wounds*, C. Springer, Editor. 2018. p. 1-41.
101. Cheng, H., et al., *Biomedical application and controlled drug release of electrospun fibrous materials.* Materials Science and Engineering: C, 2018. **90**: p. 750-763.
102. Sill, T.J. and H.A. von Recum, *Electrospinning: applications in drug delivery and tissue engineering.* Biomaterials, 2008. **29**(13): p. 1989-2006.
103. Morgado, P.I., et al., *Ibuprofen loaded PVA/chitosan membranes: A highly efficient strategy towards an improved skin wound healing.* Carbohydrate polymers, 2017. **159**: p. 136-145.
104. Ghalei, S., H. Asadi, and B. Ghalei, *Zein nanoparticle-embedded electrospun PVA nanofibers as wound dressing for topical delivery of anti-inflammatory diclofenac.* Journal of applied polymer science, 2018. **135**(33): p. 46643.
105. Park, Y.-J., et al., *Development of novel ibuprofen-loaded solid dispersion with improved bioavailability using aqueous solution.* Archives of pharmacal research, 2009. **32**(5): p. 767-772.
106. Yuan, Z., et al., *Ibuprofen-loaded electrospun fibrous scaffold doped with sodium bicarbonate for responsively inhibiting inflammation and promoting muscle wound healing in vivo.* Biomaterials Science, 2014. **2**(4): p. 502-511.
107. Morgado, P.I., et al., *Poly (vinyl alcohol)/chitosan asymmetrical membranes: Highly controlled morphology toward the ideal wound dressing.* Journal of membrane science, 2014. **469**: p. 262-271.
108. Hajiali, H., et al., *Alginate–lavender nanofibers with antibacterial and anti-inflammatory activity to effectively promote burn healing.* Journal of Materials Chemistry B, 2016. **4**(9): p. 1686-1695.
109. Kant, V., et al., *Antioxidant and anti-inflammatory potential of curcumin accelerated the cutaneous wound healing in streptozotocin-induced diabetic rats.* International immunopharmacology, 2014. **20**(2): p. 322-330.
110. Mohiti-Asli, M., et al., *Ibuprofen loaded PLA nanofibrous scaffolds increase proliferation of human skin cells in vitro and promote healing of full thickness incision wounds in vivo.* Journal of Biomedical Materials Research Part B: Applied Biomaterials, 2017. **105**(2): p. 327-339.

111. Han, G. and R. Ceilley, *Chronic wound healing: a review of current management and treatments*. Advances in therapy, 2017. **34**(3): p. 599-610.
112. Siddiqui, A.R. and J.M. Bernstein, *Chronic wound infection: facts and controversies*. Clinics in dermatology, 2010. **28**(5): p. 519-526.
113. Ranghar, S., et al., *Nanoparticle-based drug delivery systems: promising approaches against infections*. Brazilian archives of biology and technology, 2014. **57**(2): p. 209-222.
114. Burt, S., *Essential oils: their antibacterial properties and potential applications in foods—a review*. International journal of food microbiology, 2004. **94**(3): p. 223-253.
115. Brochot, A., et al., *Antibacterial, antifungal, and antiviral effects of three essential oil blends*. MicrobiologyOpen, 2017. **6**(4): p. e00459.
116. Bachir, R.G. and M. Benali, *Antibacterial activity of the essential oils from the leaves of Eucalyptus globulus against Escherichia coli and Staphylococcus aureus*. Asian pacific journal of tropical biomedicine, 2012. **2**(9): p. 739-742.
117. Liu, Q., et al., *Antibacterial and antifungal activities of spices*. International journal of molecular sciences, 2017. **18**(6): p. 1283.
118. Chouhan, S., K. Sharma, and S. Guleria, *Antimicrobial activity of some essential oils—present status and future perspectives*. Medicines, 2017. **4**(3): p. 58.
119. Woronuk, G., et al., *Biosynthesis and therapeutic properties of Lavandula essential oil constituents*. Planta medica, 2011. **77**(01): p. 7-15.
120. Akthar, M.S., B. Degaga, and T. Azam, *Antimicrobial activity of essential oils extracted from medicinal plants against the pathogenic microorganisms: a review*. Journal Issues ISSN, 2014. **2**: p. 1-7.
121. Koroch, A.R., H.R. Juliani, and J.A. Zygadlo, *Bioactivity of essential oils and their components*, in *Flavours and fragrances*. 2007, Springer. p. 87-115.
122. Bajpai, V.K., A. Sharma, and K.-H. Baek, *Antibacterial mode of action of Cudrania tricuspidata fruit essential oil, affecting membrane permeability and surface characteristics of food-borne pathogens*. Food control, 2013. **32**(2): p. 582-590.
123. Lv, F., et al., *In vitro antimicrobial effects and mechanism of action of selected plant essential oil combinations against four food-related microorganisms*. Food research international, 2011. **44**(9): p. 3057-3064.
124. Prusinowska, R. and K.B. Śmigielski, *Composition, biological properties and therapeutic effects of lavender (Lavandula angustifolia L). A review*. Herba polonica, 2014. **60**(2): p. 56-66.
125. Hajhashemi, V., A. Ghannadi, and B. Sharif, *Anti-inflammatory and analgesic properties of the leaf extracts and essential oil of Lavandula angustifolia Mill*. Journal of ethnopharmacology, 2003. **89**(1): p. 67-71.
126. Balasubramanian, K. and K.M. Kodam, *Encapsulation of therapeutic lavender oil in an electrolyte assisted polyacrylonitrile nanofibres for antibacterial applications*. Royal Society of Chemistry advances, 2014. **4**(97): p. 54892-54901.

127. Simões, D., S.P. Miguel, and I.J. Correia, *Biofunctionalization of electrospun poly (caprolactone) fibers with Maillard reaction products for wound dressing applications.* Reactive and Functional Polymers, 2018. **131**: p. 191-202.
128. Antunes, B.P., et al., *Chitosan/arginine–chitosan polymer blends for assembly of nanofibrous membranes for wound regeneration.* Carbohydrate polymers, 2015. **130**: p. 104-112.
129. Moreira, A.F., et al., *Preparation of end-capped pH-sensitive mesoporous silica nanocarriers for on-demand drug delivery.* European Journal of Pharmaceutics and Biopharmaceutics, 2014. **88**(3): p. 1012-1025.
130. Goyal, R., et al., *Nanoparticles and nanofibers for topical drug delivery.* Journal of Controlled Release, 2016. **240**: p. 77-92.
131. Zeng, J., et al., *Biodegradable electrospun fibers for drug delivery.* Journal of controlled release, 2003. **92**(3): p. 227-231.
132. Pires, L.R., et al., *Ibuprofen-loaded poly (trimethylene carbonate-co-ε-caprolactone) electrospun fibres for nerve regeneration.* Journal of tissue engineering and regenerative medicine, 2016. **10**(3): p. E154-E166.
133. Liu, S., et al., *Prevention of peritendinous adhesions with electrospun ibuprofen-loaded poly (L-lactic acid)-polyethylene glycol fibrous membranes.* Tissue Engineering Part A, 2012. **19**(3-4): p. 529-537.
134. Rajangam, K., et al., *Heparin binding nanostructures to promote growth of blood vessels.* Nano letters, 2006. **6**(9): p. 2086-2090.
135. Najafi, M., J. Chery, and M. Frey, *Functionalized Electrospun Poly (Vinyl Alcohol) Nanofibrous Membranes with Poly (Methyl Vinyl Ether-Alt-Maleic Anhydride) for Protein Adsorption.* Materials, 2018. **11**(6): p. 1002.
136. Zhai, M., et al., *Syntheses of PVA/starch grafted hydrogels by irradiation.* Carbohydrate Polymers, 2002. **50**(3): p. 295-303.
137. Carreras, N., et al., *Drug release system of ibuprofen in PCL-microspheres.* Colloid and Polymer Science, 2013. **291**(1): p. 157-165.
138. An, J., et al., *Preparation and antibacterial activity of electrospun chitosan/poly (ethylene oxide) membranes containing silver nanoparticles.* Colloid and Polymer Science, 2009. **287**(12): p. 1425-1434.
139. Morgan, T.J., et al., *Essential oils investigated by size exclusion chromatography and gas chromatography− mass spectrometry.* Energy & fuels, 2006. **20**(2): p. 734-737.
140. Sahputra, I.H., A. Alexiadis, and M.J. Adams, *Effects of Moisture on the Mechanical Properties of Microcrystalline Cellulose and the Mobility of the Water Molecules as Studied by the Hybrid Molecular Mechanics–Molecular Dynamics Simulation Method.* Journal of Polymer Science Part B: Polymer Physics, 2019. **57**(8): p. 454-464.
141. Li, Q., et al., *Genipin-crosslinked electrospun chitosan nanofibers: Determination of crosslinking conditions and evaluation of cytocompatibility.* Carbohydrate polymers, 2015. **130**: p. 166-174.

142. Jin, G., et al., *Tissue engineered plant extracts as nanofibrous wound dressing.* Biomaterials, 2013. **34**(3): p. 724-734.
143. Chong, E., et al., *Evaluation of electrospun PCL/gelatin nanofibrous scaffold for wound healing and layered dermal reconstitution.* Acta biomaterialia, 2007. **3**(3): p. 321-330.
144. Jabur, A., M. Najim, and S.A.A. Al-Rahman, *Study the effect of flow rate on some physical properties of different polymeric solutions*, in *Journal of Physics: Conference Series*. 2018, IOP Publishing. p. 012069.
145. Jannesari, M., et al., *Composite poly (vinyl alcohol)/poly (vinyl acetate) electrospun nanofibrous mats as a novel wound dressing matrix for controlled release of drugs.* International journal of nanomedicine, 2011. **6**: p. 993-1003.
146. Yap, P., et al., *Membrane disruption and anti-quorum sensing effects of synergistic interaction between L avandula angustifolia (lavender oil) in combination with antibiotic against plasmid-conferred multi-drug-resistant E scherichia coli.* Journal of applied microbiology, 2014. **116**(5): p. 1119-1128.
147. Jamróz, E., L. Juszczak, and M. Kucharek, *Investigation of the physical properties, antioxidant and antimicrobial activity of ternary potato starch-furcellaran-gelatin films incorporated with lavender essential oil.* International journal of biological macromolecules, 2018. **114**: p. 1094-1101.
148. Gudiksen, K.L., et al., *Eliminating Positively Charged Lysine E-NH3 Groups on the Surface of Carbonic Anhydrase Has No Significant Influence on Its Folding from Sodium Dodecyl Sulfate.* Journal of the American Chemical Society, 2005. **127**: p. 4707-4714.
149. Fountoulakis, M. and H.-W. Lahm, *Hydrolysis and amino acid composition analysis of proteins.* Journal of chromatography A, 1998. **826**(2): p. 109-134.
150. Adderley, U.J., *Managing wound exudate and promoting healing.* British journal of community nursing, 2010. **15**(3): p. S15-S20.
151. Harms, M.J., et al., *A buried lysine that titrates with a normal pKa: Role of conformational flexibility at the protein–water interface as a determinant of pKavalues.* Protein Science, 2008. **17**(5): p. 833-845.
152. Jesus, A.L. and J. Redinha, *Molecular insight into the amine–water interaction: A combined vibrational, energetic and NBO/NEDA study.* Computational and Theoretical Chemistry, 2013. **1023**: p. 74-82.
153. Xu, R., et al., *Controlled water vapor transmission rate promotes wound-healing via wound re-epithelialization and contraction enhancement.* Scientific reports, 2016. **6**: p. 24596.
154. Jonkman, M.F., et al., *New method to assess the water vapour permeance of wound coverings.* Biomaterials, 1988. **9**(3): p. 263-267.
155. Naseri, N., et al., *Electrospun chitosan-based nanocomposite mats reinforced with chitin nanocrystals for wound dressing.* Carbohydrate polymers, 2014. **109**: p. 7-15.

156. Arima, Y. and H. Iwata, *Effect of wettability and surface functional groups on protein adsorption and cell adhesion using well-defined mixed self-assembled monolayers.* Biomaterials, 2007. **28**(20): p. 3074-3082.
157. Oliveira, S.M., N.M. Alves, and J.F. Mano, *Cell interactions with superhydrophilic and superhydrophobic surfaces.* Journal of Adhesion Science and Technology, 2014. **28**(8-9): p. 843-863.
158. Lowe, T.L., H. Tenhu, and H. Tylli, *Effect of hydrophobicity of a drug on its release from hydrogels with different topological structures.* Journal of applied polymer science, 1999. **73**(6): p. 1031-1039.
159. Pérez, D.J., et al., *Silicon containing ibuprofen derivatives with antioxidant and anti-inflammatory activities: An in vivo and in silico study.* European journal of pharmacology, 2017. **814**: p. 18-27.
160. Costa, D., et al., *Antioxidant activity and inhibition of human neutrophil oxidative burst mediated by arylpropionic acid non-steroidal anti-inflammatory drugs.* Biological and Pharmaceutical Bulletin, 2006. **29**(8): p. 1659-1670.
161. Huang, D., B. Ou, and R.L. Prior, *The chemistry behind antioxidant capacity assays.* Journal of agricultural and food chemistry, 2005. **53**(6): p. 1841-1856.
162. Van Antwerpen, P. and J. Neve, *In vitro comparative assessment of the scavenging activity against three reactive oxygen species of non-steroidal anti-inflammatory drugs from the oxicam and sulfoanilide families.* European journal of pharmacology, 2004. **496**(1-3): p. 55-61.
163. Danh, L.T., et al., *Antioxidant activity, yield and chemical composition of lavender essential oil extracted by supercritical CO2.* The Journal of Supercritical Fluids, 2012. **70**: p. 27-34.
164. Yang, S.-A., et al., *Comparative study of the chemical composition and antioxidant activity of six essential oils and their components.* Natural product research, 2010. **24**(2): p. 140-151.
165. Kacániová, M., et al., *Antimicrobial and antiradicals activity of Origanum vulgare L. and Thymus vulgaris essential oils.* The Journal of Microbiology, Biotechnology and Food Sciences, 2012. **2**(1): p. 263-271.
166. Eça, K.S., T. Sartori, and F.C. Menegalli, *Films and edible coatings containing antioxidants-a review.* Brazilian Journal of Food Technology, 2014. **17**(2): p. 98-112.
167. Gizaw, M., et al., *Electrospun fibers as a dressing material for drug and biological agent delivery in wound healing applications.* Bioengineering, 2018. **5**(1): p. 9.
168. Negut, I., V. Grumezescu, and A. Grumezescu, *Treatment strategies for infected wounds.* Molecules, 2018. **23**(9): p. 2392.
169. Dash, S., et al., *Kinetic modeling on drug release from controlled drug delivery systems.* Acta Poloniae Pharmaceutica, 2010. **67**(3): p. 217-223.
170. Barrientos, S., et al., *Growth factors and cytokines in wound healing.* Wound repair and regeneration, 2008. **16**(5): p. 585-601.

171. Kim, Y.H., et al., *Enhancement of neuronal cell adhesion by covalent binding of poly-d-lysine*. Journal of neuroscience methods, 2011. **202**(1): p. 38-44.
172. Simões, D., et al., *Recent advances on antimicrobial wound dressing: A review*. European journal of pharmaceutics and biopharmaceutics, 2018. **127**: p. 130-141.
173. Cavanagh, H. and J. Wilkinson, *Biological activities of lavender essential oil*. Phytotherapy research, 2002. **16**(4): p. 301-308.
174. Lis-Balchin, M., *Lavender: the genus Lavandula*. 2003, CRC Press.
175. Lopez-Romero, J.C., et al., *Antibacterial effects and mode of action of selected essential oils components against Escherichia coli and Staphylococcus aureus*. Evidence-Based Complementary and Alternative Medicine, 2015. **2015**.
176. Sakkas, H., et al., *Antibacterial Efficacy of Commercially Available Essential Oils Tested Against Drug-Resistant Gram-Positive Pathogens*. Applied Sciences, 2018. **8**(11): p. 1-9.
177. Hyldgaard, M., et al., *The antimicrobial mechanism of action of epsilon-poly-l-lysine*. Applied and Environmental Microbiology, 2014. **80**(24): p. 7758-7770.

Appendix

1. Miguel, S.P., Sequeira, R.S., Moreira, A.F., Cabral, C.S.D., Mendonça, A.G., Ferreira, P., Correia, I.J. (2019). An overview of electrospun membranes loaded with bioactive molecules for improving the wound healing process. *European Journal of Pharmaceutics and Biopharmaceutics*.139,1-22.

2. Miguel, S.P., Simões, D., Moreira, A.F., Sequeira, R.S., Correia, I.J. (2018). Production and characterization of electrospun silk fibroin based asymmetric membranes for wound dressing applications. *International Journal of Biological Macromolecules*. 121, 524-535.